Master's Thesis
석사 학위논문

Synthesis, Characterization and Reactivity Control of Ni-Oxygen Adducts with Organic Substrates

Jalee Kim (김 자 이 金 慈 伊)

Department of Emerging Materials Science
신물질과학전공

DGIST

2015

Master's Thesis
석사 학위논문

Synthesis, Characterization and Reactivity Control of Ni-Oxygen Adducts with Organic Substrates

Jalee Kim (김 자 이 金 慈 伊)

Department of Emerging Materials Science
신물질과학전공

DGIST

2015

Synthesis, Characterization and Reactivity Control of Ni-Oxygen Adducts with Organic Substrates

Advisor : Professor Jaeheung Cho

Co-advisor : Professor Wonbae Jeon

by

Jalee Kim
Department of Emerging Materials Science
DGIST

A thesis submitted to the faculty of DGIST in partial fulfillment of the requirements for the degree of Master of Science in the Department of Emerging Materials Science. The study was conducted in accordance with Code of Research Ethics[1].

12. 18. 2014

Approved by

Professor Jaeheung Cho (Signature)
(Advisor)

Professor Wonbae Jeon (Signature)
(Co-Advisor)

[1] Declaration of Ethical Conduct in Research**:** I, as a graduate student of DGIST, hereby declare that I have not committed any acts that may damage the credibility of my research. These include, but are not limited to: falsification, thesis written by someone else, distortion of research findings or plagiarism. I affirm that my thesis contains honest conclusions based on my own careful research under the guidance of my thesis advisor.

Synthesis, Characterization and Reactivity Control of Ni-Oxygen Adducts with Organic Substrates

Jalee Kim

Accepted in partial fulfillment of the requirements for the degree of Master of Science.

12. 18. 2014

Head of Committee_____(인)
Prof. Jaeheung Cho

Committee Member_____(인)
Prof. Wonbae Jeon

Committee Member_____(인)
Prof. Nakcheon Jeong

MS/EM 201321004 김 자 이. Jalee Kim. Synthesis, Characterization and Reactivity Control of Ni-Oxygen Adducts with Organic Substrates. Department of Emerging Materials Science. 2015. 60p. Advisor Prof. Jaeheung Cho, Co-Advisor Prof. Wonbae Jeon.

ABSTRACT

The reactivity of mononuclear metal-O_2 adducts, such as metal-superoxo and -peroxo species, has long fascinated researchers in many areas due to the significance of diverse biological and catalytic processes. To understand how the nature of the ligand influences reactivity patterns of the metal-O_2 complexes, recently, a systematic study of the relationship between reactivity and ring size of ligand was undertaken for a series of metal-O_2 complexes bearing *N*-tetramethylated macrocyclic chelates in biomimetic chemistry. In this study, the two ligands, CHDAP and Me_3-TPADP, were designed and reactivity of Ni-O_2 species bearing each ligand was investigated in part I and part II, respectively. For comparison of reactivity according to a steric effect, a set of nickel(III)-peroxo complexes bearing tetraazamacrocyclic ligands, $[Ni^{III}(CHDAP)(O_2)]^+$ and $[Ni^{III}(TBDAP)(O_2)]^+$, were prepared and fully characterized by various physicochemical methods. The different steric properties of the supporting ligands were confirmed by X-ray crystallography where the CHDPA ligand gives enough space around the Ni-O_2 core compared to the TBDAP ligand. In the aldehyde deformylation reaction, the nucleophilic reactivity of the nicke(III)-peroxo complexes was highly dependent on the steric properties of the macrocyclic ligands, with the reactivity order of $[Ni^{III}(TBDAP)(O_2)]^+ < [Ni^{III}(CHDAP)(O_2)]^+$. This result provides fundamental insight into the mechanism of the structure (steric) – reactivity relationship of metal-peroxo intermediates. In part II, the Me_3-TPADP ligand was synthesized, and the starting complex, $[Ni^{II}(Me_3\text{-}TPADP)(CH_3CN)_2]^{2+}$ (**3**), and Ni-O_2 intermediate, $[Ni^{III}(Me_3\text{-}TPADP)(O_2)]^+$ (**4**), were prepared and successfully characterized by various methods. Also, the kinetic result of **4** was obtained with external organic substrates.

Keywords: Ni-O_2, steric effect, electronic effect, kinetic.

Contents

List of Schemes

List of Figures

List of Tables

List of Abbreviations

L1	Pyridine-2,6-dicarbaldehyde
L2	*N,N'*-(pyridine-2,6-diylbis(methylene))bis(2-cyclohexyl-2amine)
L3	2,6-bis(chloromethyl)pyridine
L4	1,4,7-tris(*p*-tosylsulfonyl)-1,4,7-triazaheptane
L5	3,6,9-tris(p-tosylsulfonyl)-3,6,9,15-tetraazbicyclo[9,3,1]pentadeca-1(15),11,13-triene
L6	3,6,9,15-tetraazabocyclo(9,3,1)pentadeca-1(15),11,13-triane
CHDAP	*N,N'*-di-cyclohexyl-2,11-diaza[3.3](2,6)-pyridinophane
TBDAP	*N,N'*-di-tert-butyl-2,11-diaza[3.3](2,6)-pyridinophane
Me_3-TPADP	3,6,9-trimethyl-3,6,9-triaza-1(2,6)-pyridinacyclodecaphane
Complex **1**	$[Ni^{II}(CHDAP)(NO_3)]^+$
Complex **2**	$[Ni^{III}(CHDAP)(O_2)]^+$
Complex **3**	$[Ni^{II}(Me_3\text{-}TPADP)(CH_3CN)_2]^{2+}$
Complex **4**	$[Ni^{III}(Me_3\text{-}TPADP)(O_2)]^+$
ESI-MS	electrospray ionization mass spectrometry
EA	Elemental Analysis
HPLC	high performance liquid chromatography
GC	gas chromatography
GC-MS	gas chromatography mass spectrometry
EPR	electron paramagnetic resonance
NMR	nuclear magnetic resonance
ORTEP	Oak Ridge Thermal Ellipsoid Plot

2-PPA	2-Phenylpropionaldehyde
CCA	Cyclohexnaecarboxaldehyde

Part I.

A Steric Effect on the Nucleophilic Reactivity of Nickel(III)-O_2 Complex

I. Introduction

Mononuclear metal-O_2 adducts, such as metal-peroxo and superoxo species, are the crucial reactive intermediates in enzymatic reactions as well as oxidative catalytic processes (Scheme 1). For example, manganese(III)-peroxo intermediates have been invoked as reactive species in manganese-containing enzymes including oxalate oxidase, catalase and superoxide dismutase.[1-3] In addition, mononuclear iron(III)-peroxo species is often observed in the activation of dioxygen by iron enzymes (*e.g.*, cytochromes P450 and Rieske dioxygenases).[4-7]

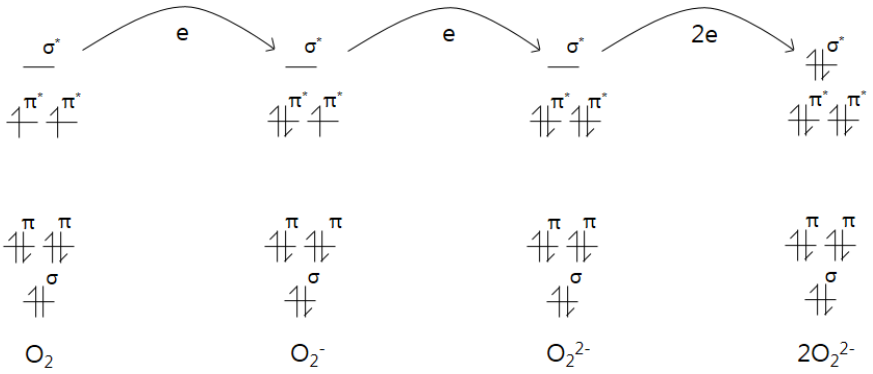

Scheme 1. Stepwise reduction process of dioxygen.

Cytochrome P450 (P450, CYP), heme proteins containing a heme cofactor, is a superfamily enzyme. Cytochrome P450 was named in the sense of pigment which exhibits a characteristic light absorption at 450 nm in combination with the CO. CYP450, known as essential catalyst enzyme to perform the oxidative metabolism for drug or lipid in our body has a proposed cycle mechanism (Scheme 2).[8] Catalytic cycle with CYP450 can be divided into several stages, substrate binding, reduction of the iron, oxygen binding, uptake of a electron, protonation to give intermediate, cleavage of oxygen-oxygen bond.[9]

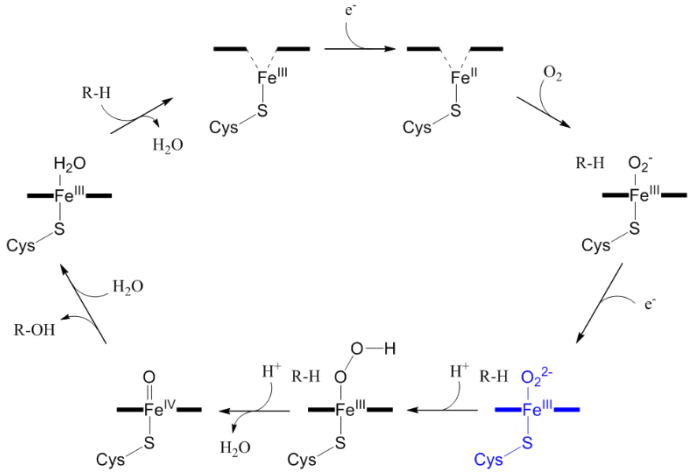

Scheme 2. Proposed catalytic mechanism of CYP 450.

Rieske dioxygenases, found in soil bacteria, catalyze the cis-dihydroxylation of polyaromatic hydrocarbons to cis-dihydro-diol that reaction is initial step of aromatic hydrocarbon biodegradation.[10] These enzymes has three components: NADH-dependent FAD reductase, a ferredoxin with two [2Fe-2S] Rieske cluster, and an α3β3 oxygenase that each α-subunit containing a [2Fe-2S] Rieske cluster and mononuclear iron active center (Scheme 3).[10a] The increase of the interest on aromatic hydrocarbon dioxygenase is due to the potential that can solve the environmental pollution, contaminated of soil and water by aromatic hydrocarbon, by using microorganisms.[10b]

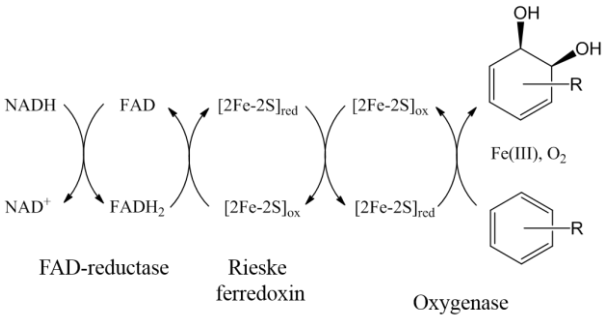

Scheme 3. Electron transfer mechanism of Rieske dioxygenases.

In synthetic model chemistry, iron(III)-peroxo complexes has been prepared and characterized with various physicochemical methods, and reactivities of the models were investigated in biomimetic reactions.[11] Many people have also reported the synthesis and spectroscopic and structural characterization of an iron(III)-peroxo complex, $[Fe^{III}(TMC)(O_2)]^+$, which is capable of conducting aldehyde deformylation,[12,13] and highlighted its unique conversion procedures; upon protonation, the iron(III)-peroxo complex is converted to an iron(III)-hydroperoxo complex, which readily undergoes O-O bond cleavage affording the formation of an iron(IV)-oxo complex.[13,14]

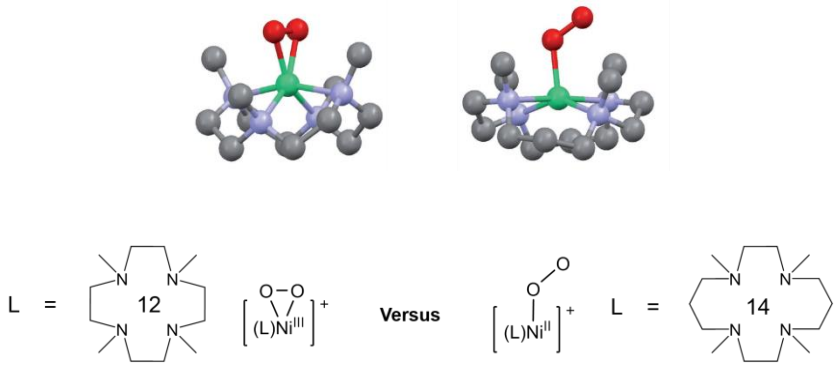

Scheme 4. Formation of Ni(III)-peroxo versus Ni(II)-superoxo intermdiates and schematic showing the [NiIII(12-TMC)(O2)]+ (left) and [NiII(14-TM)(O2)]+ (right). (12-TMC = 1,4,7,10-tetra-methyl-1,4,7,10-tetraazacyclotetradecane, 14-TMC = 1,4,8,11-tetra-methyl-1,4,8,11-tetraazacyclotetradecane)

Recent advances in biomimetic chemistry have a chance to generate a series of mononuclear side-on metal(III)-peroxo complexes bearing *N*-tetramethylated macrocyclic ligands where the spectroscopic properties and reactivities of the metal(III)-peroxo species are profoundly affected by the ring size effect of the supporting ligands.[15-17] Notable example is the formation of a side-on nickel(III)-peroxo complex with the 12-membered macrocycle and an end-on nickel(II)-superoxo complex bearing the 14-membered macrocycle (Scheme. 4).[18,19] The former has a nucleophilic character (*e.g.*, aldehyde deformylation) while the latter shows

electrophilic reactivity (*e.g.*, phosphine oxidation) toward organic substrates. The ring size effect in these studies does result in significant changes on the structures formed and reactivity patterns of the nickel-O_2 species. However, the ring size effect in this and many other cases is potentially ambiguous with respect to distinguish between influences from steric vs electronic factors.[15-20]

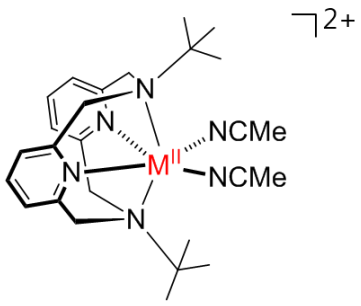

$M^{II} = Fe^{II}, Co^{II}, Ni^{II}, Cu^{II}$

Scheme 5. Pyridinophane ligand, TBDAP, with vaious metal.

It is necessary to understand the role of controlling factors related on the nature of the supporting ligand, which influences the resulting reactivity patterns. To the best of our knowledge, the steric effect has never been observed in the reactivity of mononuclear metal(III)-peroxo complexes toward external substrates, although the electronic effect on the reactivity of the nickel-alkylperoxo complex has been reported very recently.[21] Therefore, we design the CHDAP (*N,N'*-di-cyclohexyl-2,11-diaza[3,3](2,6)pyridinophane) ligand that can be expected the difference of reactivity with organic substrate cause the Ni-O_2 have a more open space according to introduction of cyclohexyl group than TBDAP (*N,N'*-di-*tert*-butyl-2,11-diaza[3,3](2,6)pyridinophane) system. TBDAP, previously synthesized pyridinophane type ligand, has been studied with various metal in mirica group (Scheme. 6).[22,23] Thus, we formed the TBDAP synthesis routes for substitute the cyclohexyl group, and then synthesized TBDAP

and CHDAP ligand. Here, we report a new set of nickel(III)-O_2 complex with CHDAP for the first time, which give structural differences in intermediate cores in comparison to nickel(III)-peroxo complex with TBDAP ligand (Scheme 4). The nickel(III)-O_2 complex, $[Ni^{III}(CHDAP)(O_2)]^+$ was characterized by a wide range of physicochemical methods. The intermediates has been employed in exploring the steric effect on reactivity of the nickel(III)-O_2 species toward organic substrates in nucleophilic reaction.

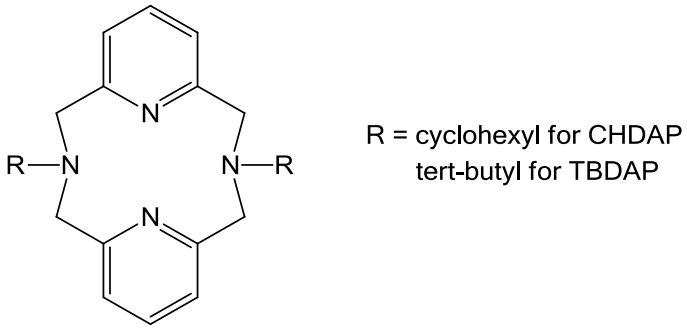

Scheme 6. Macrocyclic ligands for steric control study.

II. Experimental Section

II-1. Materials and Instrumentation

All chemicals obtained from Aldrich Chemical Co. were the best available purity and used without further purification unless otherwise indicated. Solvents were dried according to published procedures and distilled under Ar prior to use.[24] $H_2{}^{18}O_2$ (95% ^{18}O-enriched, 0.89% $H_2{}^{18}O_2$ in water) was purchased from ICON Services Inc. (Summit, NJ, USA). The TBDAP (*N,N'*-di-tert-butyl-2,11-diaza[3.3](2,6)-pyridinophane) was prepared by reacting 2,6-bis(chloromethyl)pyridine with 2,6-bis(N-t-butylamino)methyl pyridine at 80 °C.[22]

UV-vis spectra were recorded on a Hewlett Packard 8453 diode array spectrophotometer equipped with a UNISOKU Scientific Instruments for low-temperature experiments or with a circulating water bath. Electrospray ionization mass spectra (ESI-MS) were collected on a Waters (Milford, MA, USA) Acquity SQD quadrupole Mass instrument, by infusing samples directly into the source using a manual method. The spray voltage was set at 2.5 kV and the capillary temperature at 80 °C. Resonance Raman spectra were obtained using a liquid nitrogen cooled CCD detector (CCD-1024×256-OPEN-1LS, HORIBA Jobin Yvon) attached to a 1-m single polychromator (MC-100DG, Ritsu Oyo Kogaku) with a 1200 groovs/mm holographic grating. An excitation wavelength of 441.6-nm was provided by a He-Cd laser (Kimmon Koha, IK5651R-G and KR1801C), with 20 mW power at the sample point. All measurements were carried out with a spinning cell (1000 rpm) at –20 °C. Raman shifts were calibrated with indene, and the accuracy of the peak positions of the Raman bands was ±1 cm^{-1}. The effective magnetic moments was determined using the modified ^1H NMR method of Evans at room temperature.[25-27] A WILMAD® coaxial insert (sealed capillary) tubes containing the blank acetonitrile-d_3 solvent (with 1.0 % TMS) only was inserted into the normal

NMR tubes containing the complexes dissolved in acetonitrile-d_3 (with 0.03 % TMS). The chemical shift of the TMS peak (and/or solvent peak) in the presence of the paramagnetic metal complexes was compared to that of the TMS peak (and/or solvent peak) in the inner coaxial insert tube. The effective magnetic moment was calculated using the equation, $\mu = 0.0618(\Delta\nu T/2fM)^{1/2}$, where f is the oscillator frequency (MHz) of the superconducting spectrometer, T is the absolute temperature, M is the molar concentration of the metal ion, and $\Delta\nu$ is the difference in frequency (Hz) between the two reference signals. CW-EPR spectra were taken at 5 K using an X-band Bruker EMX-plus spectrometer equipped with a dual mode cavity (ER 4116DM). Low temperatures were achieved and controlled using an Oxford Instruments ESR900 liquid He quartz cryostat with an Oxford Instruments ITC503 temperature and gas flow controller. Product analysis was performed with High Performance Liquid Chromatography (HPLC, Waters Pump Series P580) equipped with a variable wavelength UV-200 detector. Quantitative analysis was made on the basis of comparison of HPLC peak integration between products and authentic samples. ^{1}H NMR and ^{13}C-NMR spectra were measured with Bruker AVANCE III-400 spectrometer.

II-2. Synthesis of Pyridinophane Type Ligands

II-2-a. Pyridine-2,6-dicarbaldehyde (L1).

We prepared **L1** by the published method.[28] 2,6-bis(hydroxymethyl)pyridine (7.5 g, 53.9 mmol) and SeO_2 (5.98 g, 53.9 mmol) in 1,4-Dioxan was refluxed 4 hours with constant stirring. The reaction mixture was filtered with celite. After the solvent remove, the remaining solid was taken up in CH_2Cl_2 and passed over a short column of silica. The final solid was collected with

evaporated, and washed with n-hexane. Yield: 5.12 g (71%), ^{1}H NMR (CDCl3, ppm): 8.07 (1H, t, PyH), 8.16 (2H, d, PyH), 10.15 (2H, s, CH)

II-2-b. *N,N'*-(pyridine-2,6-diylbis(methylene))dicyclohexylamine (L2).

To a stirred ethanol solution of **L1** (13 g, 10 mmol) was added cyclohexylamine (2.86 mL, 25 mmol) over 1 hour. Upon stirring for 6 hours, excess $NaBH_4$ was added to the mixture, which was further stirred for several hours. The solution was filtered and evaporated under reduced pressure. An ordinary work-up treatment of the reaction mixture with NaOH followed by extraction with $CHCl_3$ and evaporation gave an organic product. Yield: 2.38 g (88%), ^{1}H NMR ($CDCl_3$, 400 MHz): ~1.08 (12H, m, CH_2), ~1.70 (8H, m, CH_2), 2.40 (2H, s, CH), 3.82 (4H, s, CH_2), 7.05 (2H, d, PyH), 7.48 (1H, t, PyH).

II-2-c. 2,6-bis(chloromethyl)pyridine (L3).

To a stirred Et_2O solution of 2,6-bis(hydroxymethyl)pyridine (6.33 g) in an ice bath was slowly added thionyl chloride (7.29 mL). The mixture was then warmed on the water bath for 20 hours, during which time a white precipitate formed. The precipitate was collected by filteration. The solid was dissolved in water treated with $NaHCO_3$. The mixture was extracted with ethyl acetate. The solvent was removed under reduced pressure to yield **L3**, as a white solid. Yield: 8.82 g (91 %), ^{1}H NMR ($CDCl_3$, 400 MHz): 4.66 (4H, s, CH_2), 7.45 (2H, t, CH), 7.76 (1H, t, PyH).

II-2-d. *N,N'*-di-cyclohexyl-2,11-diaza[3,3](2,6)pyridinophane (CHDAP).

L2 (0.498 g, 2 mmol) in DMF and sodium carbonate (0.15 g) were heated at reflux. A DMF solution of **L3** (0.603 g, 3.4 mmol) was then added dropwise to the mixture over 1 hour while

stirring. After adding an ice water, a white powder precipitated and was filtered and washed with water and ethanol. Yield: 0.58 g (72%), ^{1}H NMR ($CDCl_3$, 400 MHz): δ ~1.4 (20H, m, CH_2), 2.76 (2H, t, CH), 3.92 (8H, s, CH_2), 6.72 (4H, d, PyH), 7.05 (2H, t, PyH). ^{13}C NMR ($CDCl_3$, 400 MHz): δ 159.2, 135.5, 122.5, 67.9, 60.9, 30.2, 26.6. ESI-MS (in $CHCl_3$): *m/z* 405.4 $[M + H]^+$. Anal. Calcd for $C_{26.17}H_{36.17}N_4Cl_3$ ($(CHDAP)(CHCl_3)_{1/6}$): C, 74.04; H, 8.59; N, 13.20. Found: C, 74.835; H, 8.6425; N, 13.41.

II-3. Generation of Ni Complexes

II-3-a. $[Ni(CHDAP)(NO_3)]^+$ (1).

CHDAP (0.18 g, 0.5 mmol) in chloroform (2 mL) was added to CH_3CN solution (2 mL) of $Ni(NO_3)_2{\cdot}6H_2O$ (0.15 g, 0.5 mmol). The resulting solution was stirred for 12 hours, affording a blue solution. The solvents were removed under vaccum to yield blue powder, which was recrystallized from MeOH/Et_2O solution as a blue crystalline product. Crystalline yield: 0.18 g (75%). UV-vis (CH_3CN): λ_{max} (ε) = 588 nm (15 M^{-1} cm^{-1}), 835 nm (25 M^{-1} cm^{-1}), and 1010 nm (45 M^{-1} cm^{-1}). ESI-MS (CH_3CN): *m/z* 251.7 for $[Ni(CHDAP)(CH_3CN)]^{2+}$, and 524.3 for $[Ni(CHDAP)(NO_3)]^+$. Anal. Calcd for $C_{27}H_{40}N_6O_7Ni$ ($[Ni(CHDAP)(NO_3)](NO_3)(CH_3OH)$): C, 52.36; H, 6.51; N, 13.57. Found: C, 52.28; H, 6.30; N, 13.75. μ_{eff} = 3.1 BM. X-ray crystallographically suitable crystals were obtained by slow diffusion of Et_2O into CH_3OH solution of **1**.

II-3-b. $[Ni(CHDAP)(O_2)]^+$ (2).

Treatment of $[Ni(CHDAP)(NO_3)](NO_3)(CH_3OH)$ (4 mM) with 5 equiv. H_2O_2 in the presence of 2 equiv. of TEA in CH_3CN (2 mL) at 25 ℃ afforded a green solution. Spectroscopic data,

including UV-vis, ESI-MS, resonance Raman, and EPR, were reported. $[Ni(CHDAP)(^{18}O_2)]^+$ was prepared by adding 5 equiv. of $H_2{}^{18}O_2$ (72 μL, 90% ^{18}O-enriched, 0.89% $H_2{}^{18}O_2$ in water) to a solution containing $[Ni(CHDAP)(NO_3)](NO_3)(CH_3OH)$ (4 mM) and 2 equiv. of TEA in CH_3CN (2 mL) at ambient temperature. UV-vis (CH_3CN): λ_{max} (ε) = 584 nm (35 M^{-1} cm^{-1}), 950 nm (70 M^{-1} cm^{-1}). ESI-MS (CH_3CN): 494.2 for $[Ni(CHDAP)(O_2)]^+$. μ_{eff} = 2.2 BM.

II-4. X-ray Crystallography

Single crystals of **1** was picked from solutions by a nylon loop (Hampton Research Co.) on a hand made copper plate mounted inside a liquid N_2 Dewar vessel at *ca*. –40 ℃ and mounted on a goniometer head in a N_2 cryostream. Data collections were carried out on a Bruker SMART APEX II CCD diffractometer equipped with a monochromator in the Mo Kα (λ = 0.71073 Å) incident beam. The CCD data were integrated and scaled using the Bruker-SAINT software package, and the structure was solved and refined using SHELXTL V 6.12.[29] Hydrogen atoms were located in the calculated positions. All non-hydrogen atoms were refined with anisotropic thermal parameters.

II-5. Reactivity Studies

All reactions were run in an 1-cm UV cuvette by monitoring UV-vis spectral changes of reaction solutions, and rate constants were determined by fitting the changes in absorbance at 934 nm for $[Ni^{III}(CHDAP)(O_2)]^+$ (**2**). Reactions were run at least in triplicate, and the data reported represent the average of these reactions. *In situ*-generated **2** was used in kinetic studies, such as the oxidation of 2-phenylpropionaldehyde (2-PPA) in CH_3CN/CH_3OH (1:1) at 25 ℃. After the completion of reactions, pseudo-first-order fitting of the kinetic data allowed us to determine k_{obs} values.

Products formed in the oxidation of 2-PPA by **2** in CH_3CN/CH_3OH (1:1) at 25 ℃ was analyzed by HPLC. Products was analyzed by injecting the reaction mixture directly into HPLC. Products was identified by comparing with authentic samples, and product yields were determined by comparison against standard areas prepared with authentic samples as an internal standard.

III. Results and Discussion

III-1. Synthesis and Characterization of CHDAP

The CHDAP (*N,N'*-di-cyclohexyl-2,11-diaza[3.3](2,6)-pyridinophane) was prepared by a modification of the reported procedure (Scheme 7).[28] The cycle compound of pyridinophane type, introduced the cyclohexyl group, was synthesized through the newly developed synthetic routes of the ligand. This method showed a high yield than the previously reported method. The ESI-MS for the CHDAP was detected with $CHCl_3$ solvent and has sharp peak at *m/z* of 405.4 (Fig. 1). The peak of CHDAP was analyzed out $[CHDAP + H]^+$ and inset shows an isotope distribution pattern.

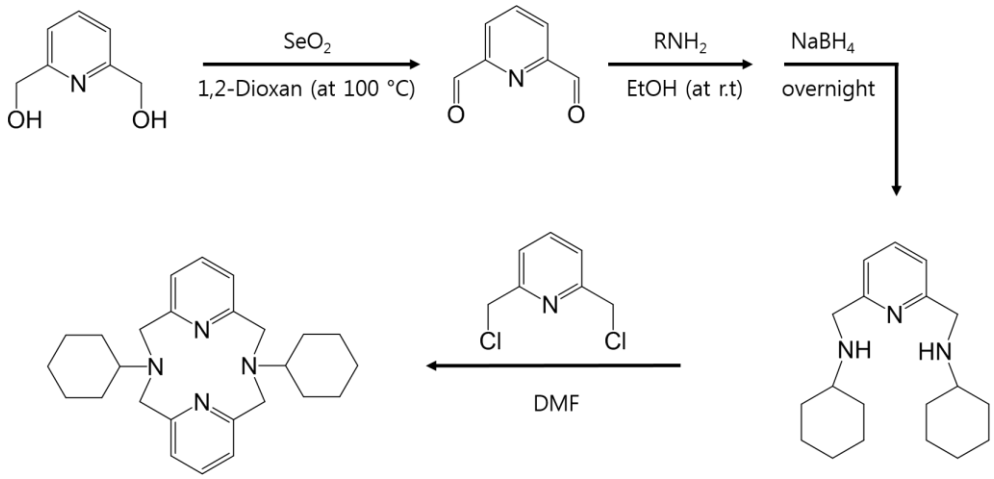

Scheme 7. Synthetic routes for CHDAP.

The CHDAP ligand was characterized by ^1H and ^{13}C NMR methods (Fig. 2 and 3). The ligand of white powder was dissolved in $CDCl_3$. The ^1H NMR of CHDAP ligand shows the Fig. 2.

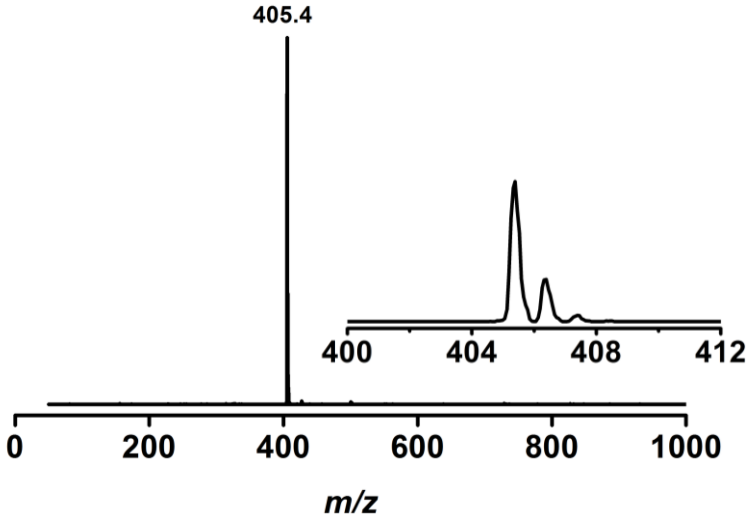

Figure 1. ESI-MS for the CHDAP ligand in $CHCl_3$. Inset shows an observed isotope distribution pattern for $[CHDAP + H]^+$.

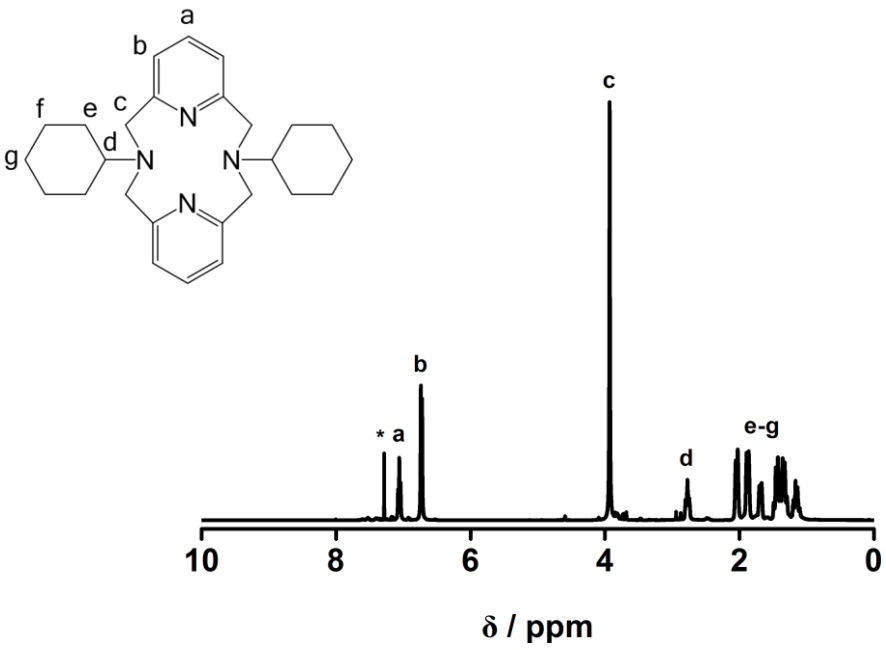

Figure 2. ^1H NMR spectrum of the CHDAP ligand in $CDCl_3$ at room temperature. The asterisk is a solvent band.

The ^{13}C NMR data for the CHDAP ligand was obtained as 159.2, 135.5, 122.5, 67.9, 30.2, 26.6 ppm (Fig. 3). The ligand confirmed to $C_{26.17}H_{36.17}N_4Cl_3$ ($(CHDAP)(CHCl_3)_{1/6}$) by elemental analysis (Anal. Calcd for ligand: C, 74.04; H, 8.59; N, 13.20. Found: C, 74.835; H, 8.6425; N, 13.41).

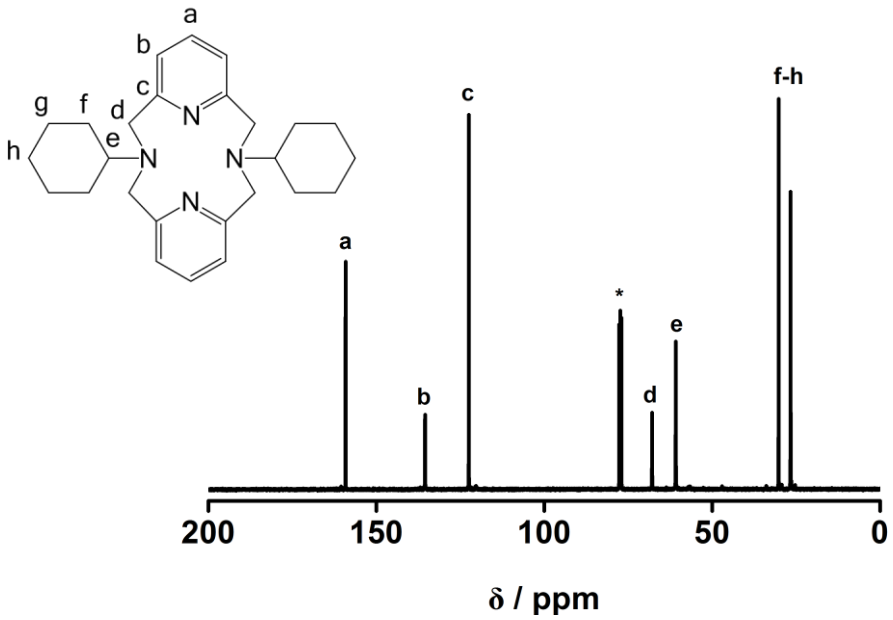

Figure 3. ^{13}C NMR spectrum of the CHDAP ligand in $CDCl_3$ at room temperature. The asterisk is a solvent band.

III-2. Preparation and Characterization of $[Ni^{II}(CHDAP)(NO_3)]^+$ (1)

The starting nickel complexes, $[Ni^{II}(CHDAP)(NO_3)]^+$, was prepared by reacting $Ni(NO_3)_2{\cdot}6H_2O$ with the CHDAP ligands at room temperature. The UV-vis spectrum of $[Ni^{II}(CHDAP)(NO_3)]^+$ in CH_3CN shows three absorption bands at 589 nm (ε = 15 M^{-1} cm^{-1}), 835 nm (ε = 25 M^{-1} cm^{-1}) and 1016 nm (ε = 45 M^{-1} cm^{-1}) (Fig. 6).

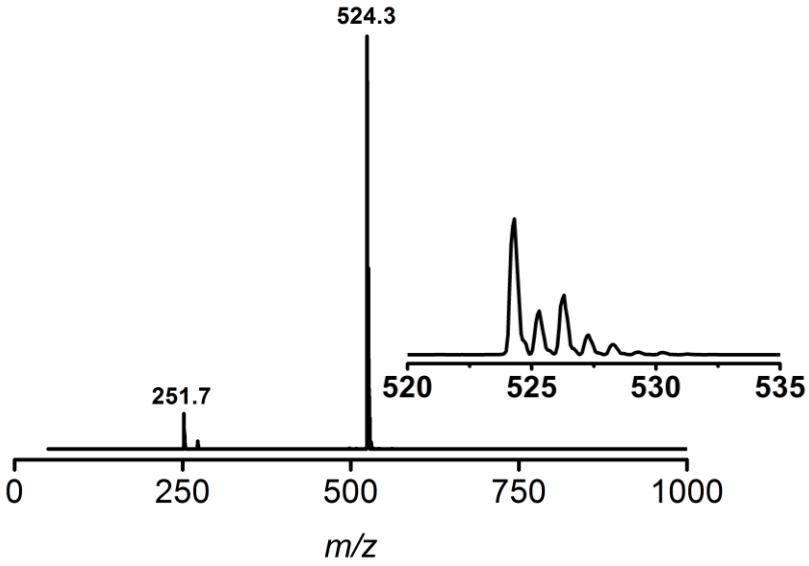

Figure 4. ESI-MS for $[Ni^{II}(CHDAP)(NO_3)]^+$ in CH_3CN. Mass peaks at 251.7 and 524.3 are assigned to $[Ni(CHDAP)(CH_3CN)]^{2+}$ and $[Ni(CHDAP)(NO_3)]^+$, respectively.

The complex **1** was recrystallized with MEOH/Et_2O solution that blue crystal in CH_3CN was confirmed by ESI-MS (Fig. 4). The ESI-MS of $[Ni^{II}(CHDAP)(NO_3)]^+$ exhibits two intense ion peaks at *m/z* of 251.7 and 524.3, whose mass and isotope distribution pattern correspond to $[Ni(CHDAP)(CH_3CN)]^{2+}$ (calculated *m/z* of 251.6) and $[Ni(CHDAP)(NO_3)]^+$ (calculated *m/z* of 524.2), respectively.

The blue crystal of **1** was recrystallized from MEOH/Et_2O solution. The molecular structure of the cationic part for $[Ni(CHDAP)(NO_3)](NO_3)(CH_3OH)$ is shown in Fig. 5, and selected bond lengths and angles are listed in Table 1 and 2. The complex has a six-coordinated Ni(II) ion with the CHDAP ligand and a symmetrically coordinated bidentate nitrate anion.

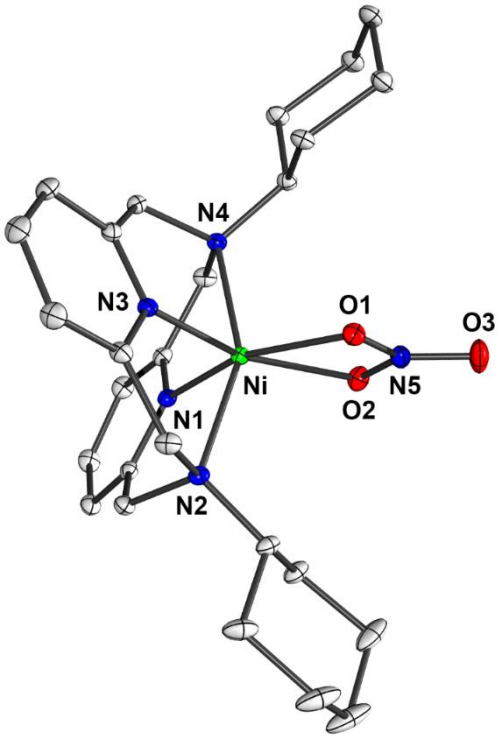

Figure 5. ORTEP plot of $[Ni(CHDAP)(NO_3)]^+$ with thermal ellipsoid drawn at the 30% probability level. Hydrogen atoms are omitted for clarity.

Crystal data for $[Ni(CHDAP)(NO_3)](NO_3)(CH_3OH)$: $C_{27}H_{40}N_6NiO_7$, Triclinic, $P\bar{1}$, Z = 2, a = 10.6798(2), b = 11.8168(2), c = 12.9559(2) Å , α = 64.1040(10), β = 82.1330(10), γ = 78.9810(10)°, V = 1441.11(4) Å ^{3}, μ = 0.729 mm^{-1}, ρ_{calcd} = 1.427 g/cm^3, R_1 = 0.0261, wR_2 = 0.0702 for 7001 unique reflections, 372 variables. CCDC-1026817 for $[Ni(CHDAP)(NO_3)](NO_3)(CH_3OH)$ contain the supplementary crystallographic data for this paper. This data can be obtained free of charge via www.ccdc.cam.ac.uk/data_request/cif (or from the Cambridge Crystallographic Data Centre, 12, Union Road, Cambridge CB2 1EZ, UK; fax: (+44) 1223-336-033; or deposit@ccdc.cam.ac.uk).

Table 1. Crystal data and structure refinements for [Ni(CHDAP)(NO_3)](NO_3)(CH_3OH).

	[Ni(CHDAP)(NO_3)](NO_3)(CH_3OH)
Empirical formula	$C_{27}H_{40}N_6NiO_7$
Formula weight	619.36
Temperature (K)	100(2)
Wavelength (Å)	0.71073
Crystal system/space group	Triclinic, $P\bar{1}$
Unit cell dimensions	
a (Å)	10.6798(2)
b (Å)	11.8168(2)
c (Å)	12.9559(2)
α (°)	64.1040(10)
β (°)	82.1330(10)
γ (°)	78.9810(10)
Volume (Å^3)	1441.11(4)
Z	2
Calculated density (g/cm^{-3})	1.427
Absorption coefficient (mm^{-1})	0.729
Reflections collected	24970
Independent reflections [R(int)]	7001 [0.0187]
Refinement method	Full-matrix least-squares on F^2
Data/restraints/parameters	7001/0/372
Goodness-of-fit on F^2	1.037
Final R indices [$I > 2$sigma(I)]	$R_1 = 0.0261$, $wR_2 = 0.0702$
R indices (all data)	$R_1 = 0.0274$, $wR_2 = 0.0713$
Largest difference peak and hole (e/Å^3)	0.521 and -0.242

Table 2. Selected bond distances (Å) and angles (º) for [Ni(CHDAP)(NO_3)](NO_3)(CH_3OH).

Bond Distances (Å)	
Ni1-N1	1.9512(9)
Ni1-N2	2.1889(9)
Ni1-N3	1.9429(9)
Ni1-N4	2.2058(9)
Ni1-O1	2.1352(8)
Ni1-O2	2.0951(8)
Bond Angles (º)	
N1-Ni1-N2	82.32(4)
N1-Ni1-N3	95.64(4)
N1-Ni1-N4	79.40(4)
N2-Ni1-N3	80.42(4)
N2-Ni1-N4	153.22(4)
N3-Ni1-N4	82.08(4)

III-3. Characterization and Reactivity Studies of $[Ni^{III}(CHDAP)(O_2)]^+$ (2)

$[Ni^{III}(CHDAP)(O_2)]^+$ (**2**) was prepared by adding 5 equiv. of H_2O_2 to a reaction solution containing **1** in the presence of 2 equiv. of triethylamine (TEA) in CH_3CN at 25 ºC; the color of the solution changed from blue to green. The UV-vis spectrum of intermediate in CH_3CN at 25 ºC shows obvious absorption bands, 584 nm (ε = 35 M^{-1} cm^{-1}) and 950 nm (ε = 70 M^{-1} cm^{-1}) (Fig. 6).

The ESI-MS data of intermediate was able to isolate more cleanly by anion substitution. Complex **2** shows a prominent signal at *m/z* of 494.2 (Fig. 7), whose mass and isotope distribution pattern correspond to $[Ni(CHDAP)(O_2)]^+$ (calculated *m/z* of 494.2). The isotope labeling experiment with $H_2{}^{18}O_2$ exhibited the expected signal at *m/z* of 498.2 for $[Ni(CHDAP)(^{18}O)]^+$ (calculated *m/z* of 498.2) (Fig. 7, inset).

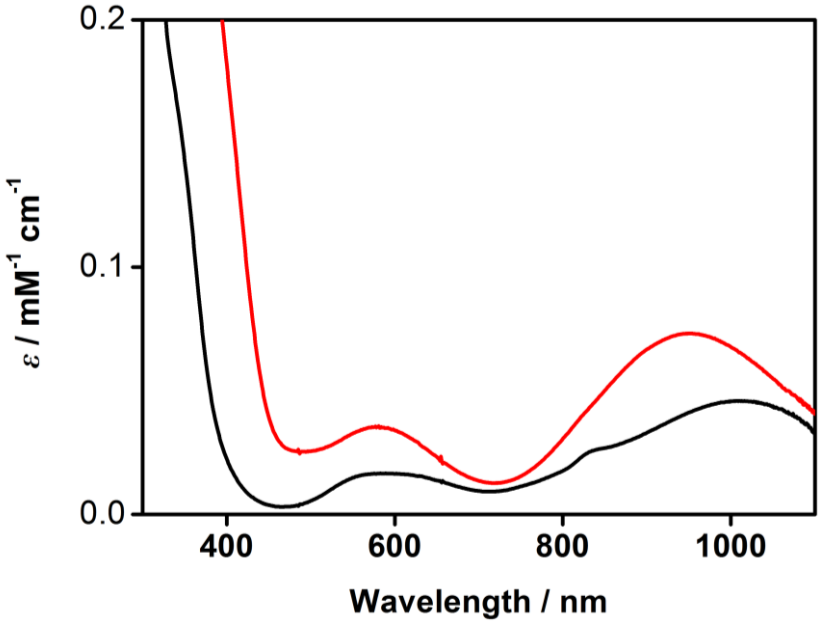

Figure 6. UV-vis spectra of $[Ni^{II}(CHDAP)(NO_3)]^+$ (**1**) (black line) and $[Ni^{III}(CHDAP)(O_2)]^+$ (**2**) (red line) in CH_3CN at 25 °C. The formation of **2** was prepared by adding 5 equiv. of H_2O_2 to a reaction solution containing **1** in the presence of 2 equiv. of triethylamine (TEA).

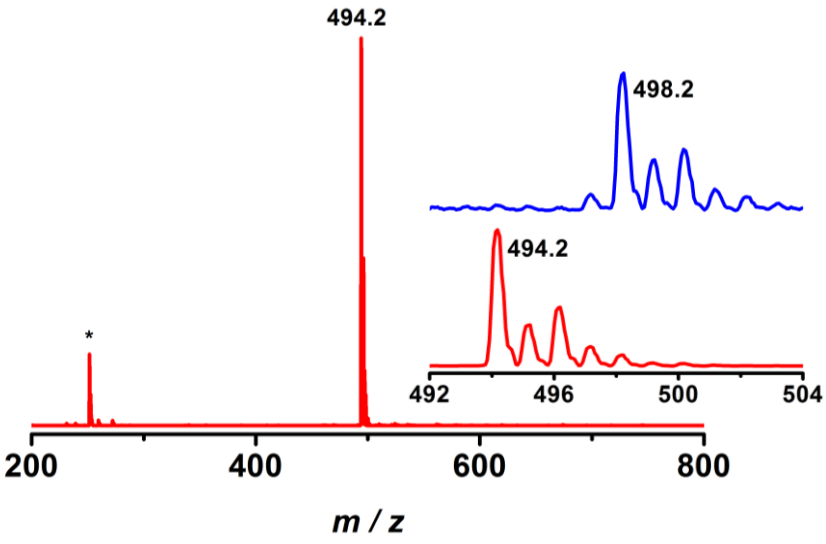

Figure 7. ESI-MS of **2** in CH_3CN at **–**20 °C. The minor peak at *m/z* 251.6 labeled with an asterisk is assignable to $[Ni(CHDAP)(CH_3CN)]^{2+}$. Insets show the observed isotope distribution patterns for $[Ni(CHDAP)(^{16}O_2)]^+$ (lower) and $[Ni(CHDAP)(^{18}O_2)]^+$ (upper).

On 442 nm excitation at –20 °C, the resonance Raman spectrum of ^{16}O-labeled **2** in CH_3CN exhibits an isotopically sensitive band at 988 cm^{-1}, which shifts to 919 cm^{-1} on ^{18}O-substitution (Fig. 8). This value is comparable to those reported for side-on Ni(III)-peroxo complexes, such as $[Ni(12\text{-}TMC)(O_2)]^+$ (1002 cm^{-1}) and $[Ni(13\text{-}TMC)(O_2)]^+$ (1008 cm^{-1}),[15c,18] indicating the peroxo character of the O_2 unit in **2**.

The EPR spectrum of a frozen CH_3CN solution of **2** at 5 K shows an axial signal with *g* values of 2.17 and 2.03 (Fig. 9), which is a typical $(d_z^2)^1$ electron configuration observed for Ni(III) complexes.[30] The room temperature magnetic moment of 2.2 μ_B,[20] determined using the ^1H NMR Evans method, is consistent with an S =1/2 ground state of **2**. The similarity of these spectroscopic features to those of 2.2 μ_B leads us to assign **2** as a side-on nickel(III)-peroxo complex.

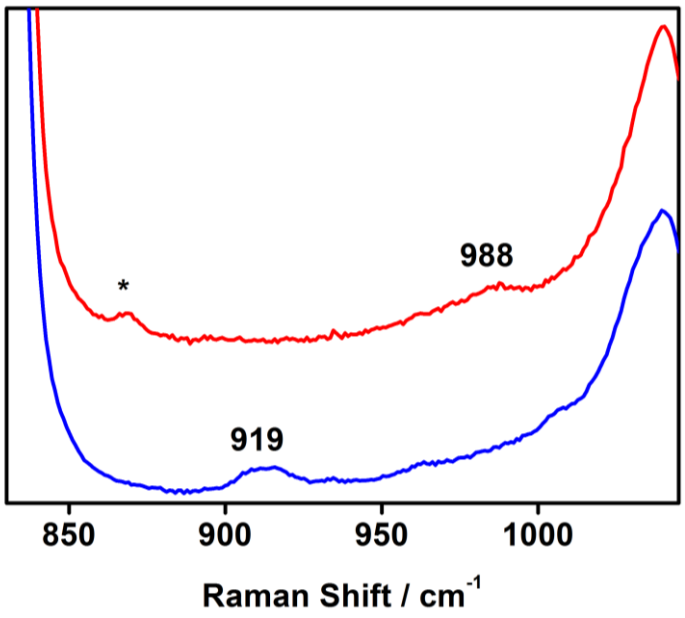

Figure 8. Resonance Raman spectra of **2** (32 mM) obtained upon excitation at 442 nm in CD_3CN at –20 °C; **2** prepared with $H_2{}^{16}O_2$ (red line) and $H_2{}^{18}O_2$ (blue line). An asterisk indicates the peak of H_2O_2.

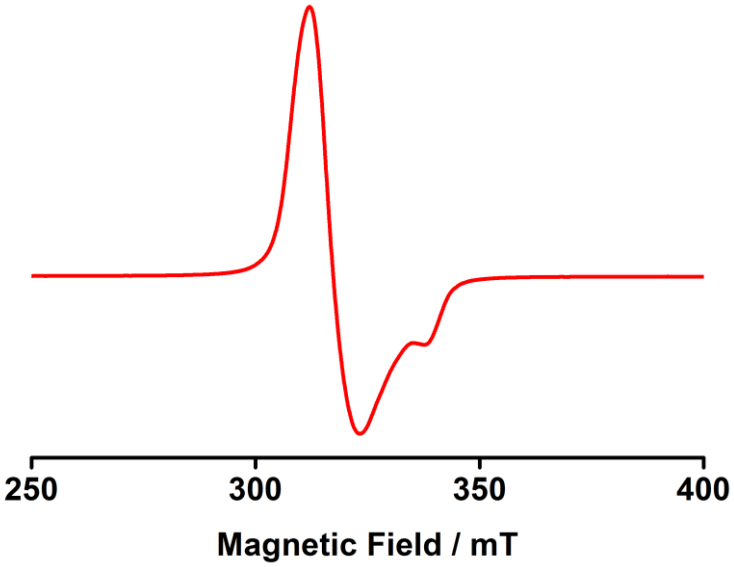

Figure 9. X-band EPR spectrum of **2** in frozen CH_3CN at 5 K. Instrumental parameters: microwave power = 1 mW, frequency = 9.646 GHz, sweep width = 0.15 T, modulation amplitude = 1 mT.

It has been noted that mononuclear metal-peroxo species react with aldehydes to give the corresponding deformylated products.[5,31-33] In order to investigate the steric effect on the reactivity of metal-peroxo species, we carried out the reaction of 2-PPA with **2**. After the intermediate generated in CH_3CN solvent at room temperature, the solution mixed 1:1 with CH_3OH immediately. Upon addition of 2-PPA to **2** in CH_3CN:CH_3OH (1:1) at 25 ^oC, the characteristic UV-vis absorption bands of **2** disappeared with pseudo-first-order decay (Fig. 10). UV-vis spectral changes of $[Ni^{III}(CHDAP)(O_2)]^+$ (**2**) (2 mM) upon addition of 100 equiv. of 2-PPA in CH_3CN:CH_3OH (1:1) at 25 ^oC. Inset shows the time course of the absorbance at 934 nm.

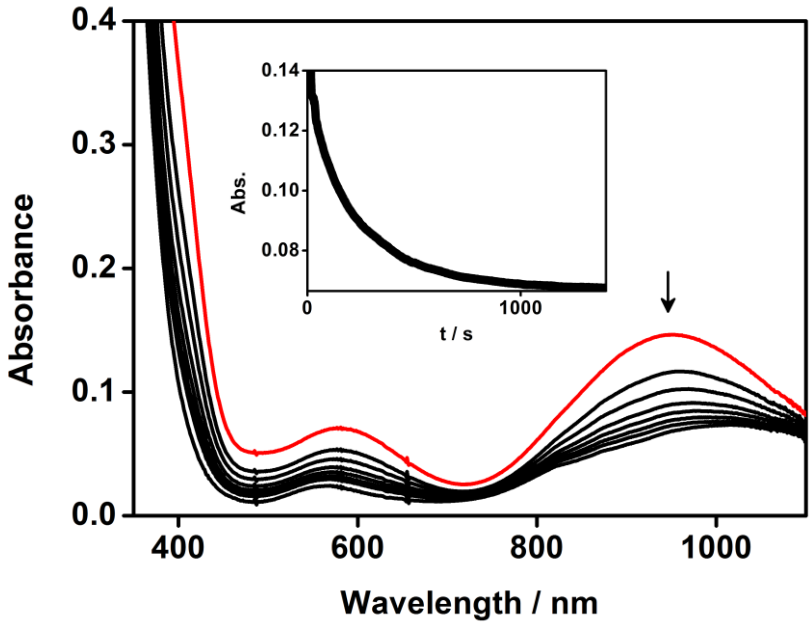

Figure 10. UV-vis spectral changes of $[Ni^{III}(CHDAP)(O_2)]^+$ (**2**) (2 mM) upon addition of 100 equiv. of 2-phenylpropionaldehyde (2-PPA) in CH_3CN:CH_3OH (1:1) at 25 °C. Inset shows the time course of the absorbance at 934 nm.

The pseudo-first-order rate constants, monitored at 934 nm, increased proportionally with the increase of the concentration of 2-PPA affording a second-order rate constant (k_2) of 6.2×10^{-2} M^{-1} s^{-1} at 25 °C (Fig. 11). Rate constant was the average obtained through more than three times of repeated experiments. When using the cyclohexanecarboxaldehyde (CCA) for kinetic study, the initial reaction was incredibly fast so this result was no longer able to be compared with the TBDAP ligand system. For the comparable system with TBDAP ligand, the appropriate conditions of CHDAP and TBDAP were identified through a numerous experiments.

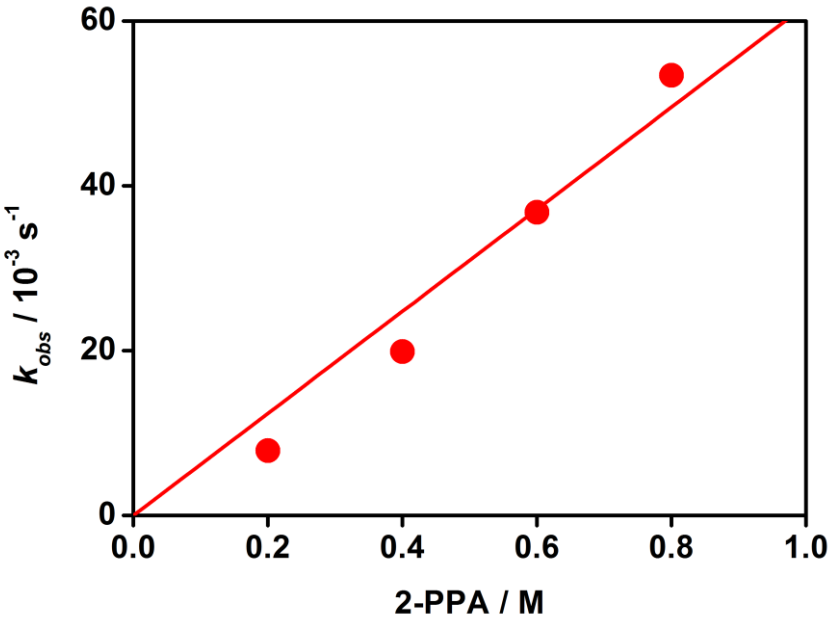

Figure 11. Plots of k_{obs} against 2-PPA concentration to determine a second-order rate constants at 25 °C.

Activation parameters for the aldehyde deformylation of **2** between 268 and 298 K were determined to be $\Delta H^{\ddagger}$ = 66 kJ mol^{-1} and $\Delta S^{\ddagger}$ = –48 J mol^{-1} K^{-1} (Fig. 12). Product analysis of the reaction solution revealed that acetophenone (90 ± 5%) was produced in the oxidation of 2-PPA. The reaction of **2** with *para*-substituted benzaldehydes, which have electron–donating and –withdrawing substituents at the *para*-position of the phenyl group (*para*-X-Ph-CHO; X = Me, F, H, Cl, Br), provides mechanistic insight into the nature of the peroxo group in **2**. The Hammett plot of log k_2 vs σ_p^+ afforded a ρ value of 1.2 (Fig. 13), which is consistent with the nucleophilic character of **2** in the oxidation of aldehydes.

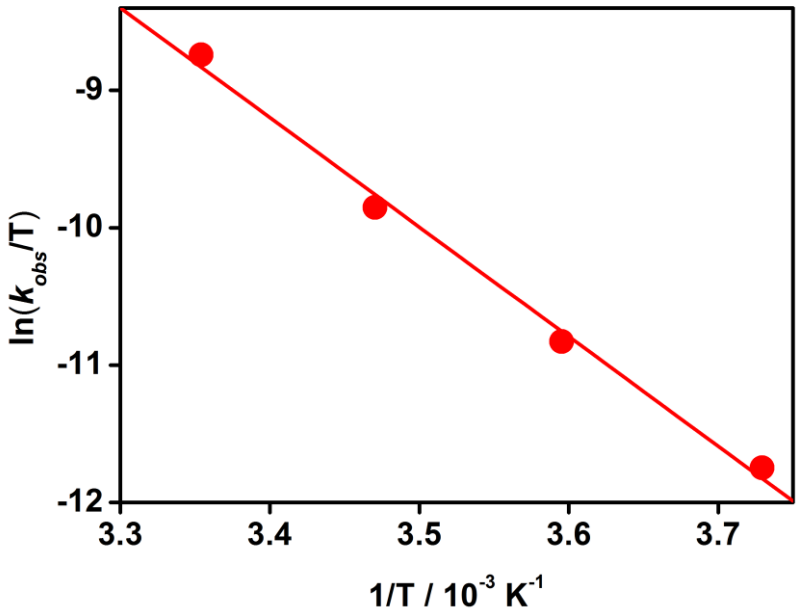

Figure 12. Plot of first-order rate constants against 1/*T* to determine activation parameters.

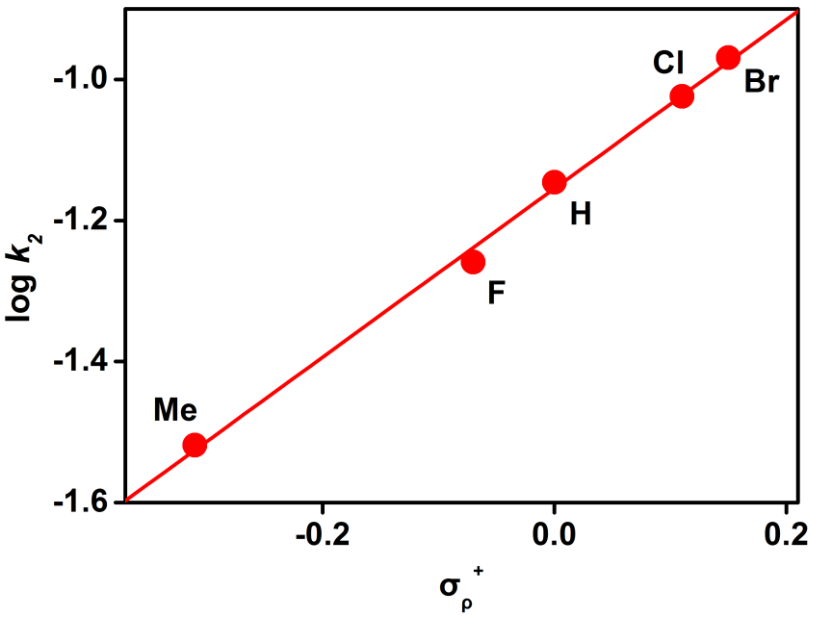

Figure 13. Hammett plot of logk_2 against σ_p^+ of *para*-substituted benzaldehydes, *para*-X-Ph-CHO (X = Me, F, H, Cl, Br), by $[Ni^{III}(CHDAP)(O_2)]^+$ (**2**) at 25 ^oC.

III-4. Comparison with Ni Complex bearing TBDAP Ligand

Synthetic procedures for Ni-O_2 complexes bearing CHDAP and TBDAP ligands are illustrated in Scheme 6. $[Ni^{III}(TBDAP)(O_2)]^+$ (**1**) was prepared by adding 5 equiv. of H_2O_2 to a reaction solution containing $[Ni^{II}(TBDAP)(NO_3)]^+$ in the presence of 2 equiv. of triethylamine (TEA) in CH_3CN at 25 °C; the color of the solution changed from blue to green.[34]

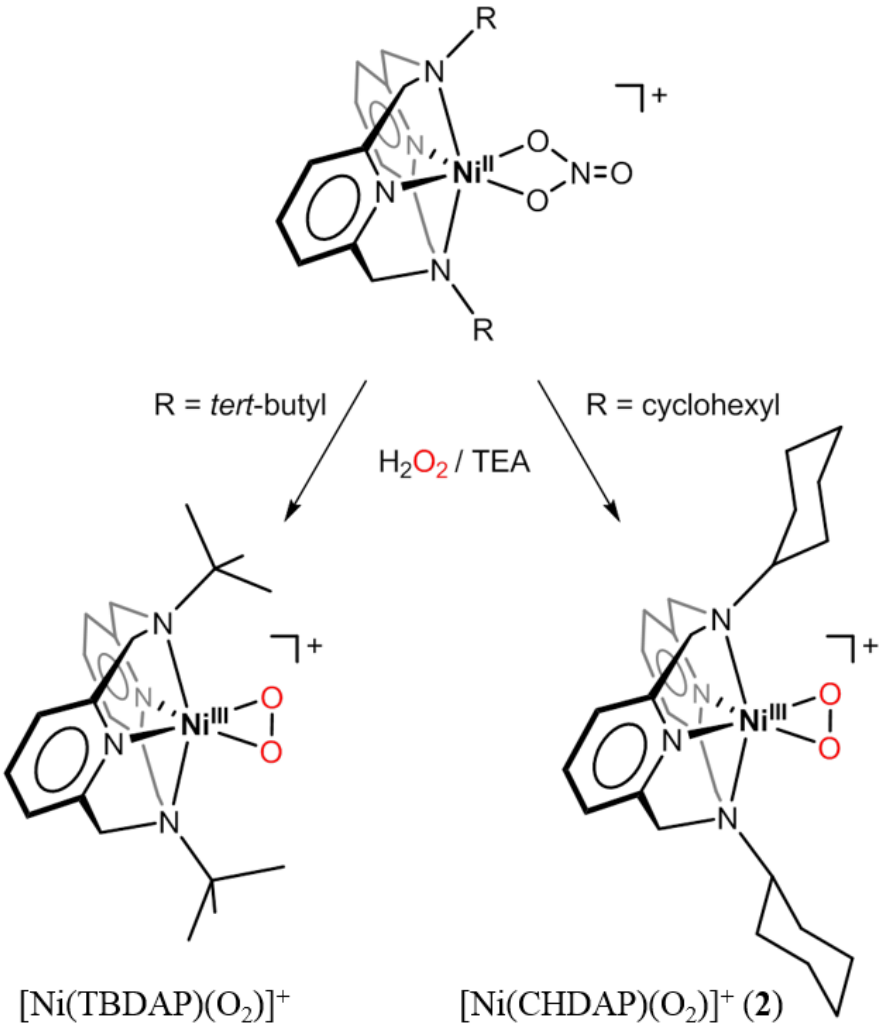

Scheme 7. Synthetic procedures for mononuclear nickel(III)-peroxo complexes.

The resonance Raman spectrum of $[Ni^{III}(TBDAP)(O_2)]^+$ collected using 442 nm excitation in CD_3CN at –20 °C shows a resonance-enhanced vibration at 989 cm^{-1} which is tentatively assigned to ν(O-O) based on its frequency and a good correlation between the O-O

bond length and O-O stretching frequency of $[Ni^{III}(TBDAP)(O_2)]^+$ (*vide infra*).[35] This result is match for complex **2**. In addition, almost identical O-O stretching frequencies of **2** (988 cm^{-1}) and $[Ni^{III}(TBDAP)(O_2)]^+$ (989 cm^{-1}) suggest that the electronic effect of *tert*-butyl and cyclohexyl groups on the NiO_2 cores is negligible.

Reacting $[Ni^{III}(TBDAP)(O_2)]^+$ with 2-PPA, the characteristic UV-vis absorption bands of $[Ni^{III}(TBDAP)(O_2)]^+$ disappeared with a pseudo-first-order decay, and product analysis of the reaction solutions revealed the formation of acetophenone (75%) in the oxidation of 2-PPA. The pseudo-first-order rate constants increased proportionally with substrate concentration, in which second-order rate constant (k_2 = 7.4 × 10^{-3} M^{-1} s^{-1} at 25 °C) was determined. The activation parameters were determined to be $\Delta H^{\ddagger}$ = 67 kJ mol^{-1} and $\Delta S^{\ddagger}$ = –62 J mol^{-1} K^{-1}. The effects of *para*-substituents on the benzaldehyde oxidation process were investigated. Hammett plot of $\ln k_{rel}$ against σ_p^+ afforded a ρ value of 7.4. The k_{rel} values were calculated by dividing k_{obs} of *para*-X-Ph-CHO (X = Me, F, H, Cl, Br) by k_{obs} of benzaldehyde at 25 °C. The positive value is consistent with the process involving a nucleophilic character. The complex **2** was calculated as ρ value of 2.8 by pseudo-first-order rate constants vs σ_p^+.

By comparing the kinetic data of **2** (k_2 = 6.2 × 10^{-2} M^{-1} s^{-1}) and $[Ni^{III}(TBDAP)(O_2)]^+$ (k_2 = 7.4 × 10^{-3} M^{-1} s^{-1}) in the oxidation of 2-PPA (Fig. 14), the reactivity of **2** is greater than that of $[Ni^{III}(TBDAP)(O_2)]^+$ in aldehyde deformylation reaction. The differential reactivity is attributable to the structural features of **2** and $[Ni^{III}(TBDAP)(O_2)]^+$ (Fig.20). The *tert*-butyl groups of $[Ni^{III}(TBDAP)(O_2)]^+$ provide the steric hindrance of the NiO_2 moiety. However, the cyclohexyl groups of **2** gives sufficient space around the NiO_2 core to allow the substrate to approach the peroxo moiety.[36] These results were also elucidated by the difference of the enthalphy values of 66 kJ mol^{-1} for **2** and 67 kJ mol^{-1} for $[Ni^{III}(TBDAP)(O_2)]^+$, and the difference of $\Delta\Delta G^{\ddagger}$ between **2** and $[Ni^{III}(TBDAP)(O_2)]^+$ is 5 kJ mol^{-1}. In addition, almost

identical O-O stretching frequencies of **2** (988 cm^{-1}) and $[Ni^{III}(TBDAP)(O_2)]^+$ (989 cm^{-1}) suggest that the electronic effect of cyclohexyl and *tert*-butyl groups on the NiO_2 cores is negligible. Consequently, by controlling the steric factor from *tert*-butyl groups to cyclohexyl groups, the aldehyde deformylation reaction by the nickel(III)-peroxo complexes is facilitated and the reaction rate is enhanced ~8 times.

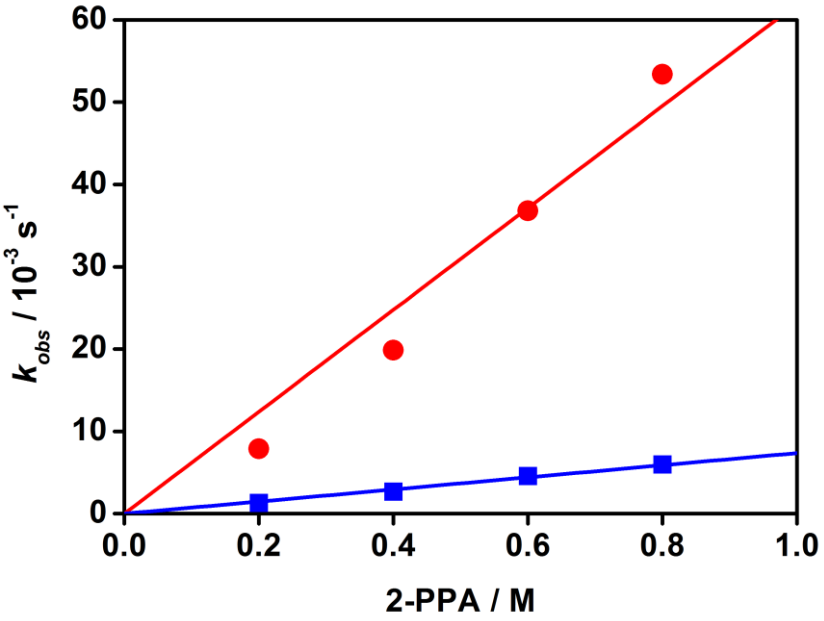

Figure 14. Kinetic studies of the reactions of $[Ni^{III}(CHDAP)(O_2)]^+$ (**2**) and $[Ni^{III}(TBDAP)(O_2)]^+$ with 2-PPA in CH_3CN:CH_3OH (1:1) at 25 °C. Plots of k_{obs} against 2-PPA concentration to determine a second-order rate constants for the reactions of **2** (●) and $[Ni^{III}(TBDAP)(O_2)]^+$ (■).

IV. Conclusion

The structure and reactivity of metal-O_2 adducts in the oxidation of organic compounds are of crucial interest in enzymatic activity, organic synthesis and industrial catalysis. A number of metal(III)-peroxo complexes and their reactivity in aldehyde deformylation have been investigated. However, the steric effect on the reactivity of metal(III)-peroxo species has not been reported yet. In this thesis, CHDAP (*N,N'*-di-cyclohexyl-2,11-diaza[3.3](2,6)-pyridinophane), macrocyclic tetradentate N_4 ligand, was successfully synthesized and characterized. The mononuclear nickel(II) complex bearing CHDAP, $[Ni^{II}(CHDPA)(NO_3)]^+$ (**1**), was well prepared and characterized with UV-vis, ESI-MS, X-ray, ^{1}H NMR of Evans, and EA methods. The intermediates, $[Ni^{III}(CHDPA)(O_2)]^+$ (**2**) was fully characterized with various physicochemical methods such as UV-vis, ESI-MS, resonance Raman, EPR and X-ray analysis. We identified that there is no electronic differences between **2** and $[Ni^{III}(TBDAP)(O_2)]^+$ according to a similar value of resonance Raman with the $H_2{}^{16}O_2$. Both **2** and $[Ni^{III}(TBDAP)(O_2)]^+$ are capable of deformylating aldehydes and the nucleophilic character of **2** and $[Ni^{III}(TBDAP)(O_2)]^+$ was confirmed by positive Hammett ρ values, which were obtained in the reaction of **2** and $[Ni^{III}(TBDAP)(O_2)]^+$ with *para*-substituted benzaldehydes. Comparison of the reactivity of **2** and $[Ni^{III}(TBDAP)(O_2)]^+$ in aldehyde deformylation reveals that the reactivity of **2** is ~8 times greater than that of $[Ni^{III}(TBDAP)(O_2)]^+$. The results regarding the disparate steric effects of the cyclohexyl groups for **2** and *tert*-butyl groups for $[Ni^{III}(TBDAP)(O_2)]^+$ are verified by spectroscopic and kinetic studies combined with structural analyses. In addition, these consequence support the complex **2** have structually more open space than $[Ni^{III}(TBDAP)(O_2)]^+$.

V. References

[1] (*a*) O. Opaleye, R.-S. Rose, M. M. Whittaker, E.-J. Woo, J. W. Whittaker and R. W. Pickersgill. (2006). "Structural and Spectroscopic Studies Shed Light on the Mechanism of Oxalate Oxidase." *J. Biol. Chem.,* **281**, 6428–6433; (*b*) T. Borowski, A. Bassan, N. G. J. Richards and P. E. M. Siegbahn. (2005). "Catalytic Reaction Mechanism of Oxalate Oxidase (Germin). A Hybrid DFT Study." *J. Chem. Theory Comput.*, **1**, 686–693.

[2] A. J. Wu, J. E. Penner-Hahn and V. L. Pecoraro. (2004). "Structural, Spectroscopic, and Reactivity Models for the Manganese Catalases." *Chem. Rev.*, **104**, 903–938.

[3] (*a*) L. E. Grove and T. C. Brunold. (2008). "Second-Sphere Tuning of the Metal Ion Reduction Potentials in Iron and Manganese Superoxide Dismutases." *Comments Inorg. Chem.*, **29**, 134–168; (*b*) A.-F. Miller. (2004). "Superoxide dismutases: active sites that save, but a protein that kills." *Curr. Opin. Chem. Biol.*, **8**, 162–168; (*c*) T. A. Jackson, A. Karapetian, A.-F. Miller and T. C. Brunold. (2005). "Probing the Geometric and Elecgtronic Structures of the Low-Temperature Azide Adduct and the Product-Inhibited Form of Oxidized Manganese Superoxide Dismutase." *Biochemistry*, **44**, 1504–1520; (*d*) C. Bull, E. C. Niederhoffer, T. Yoshida and J. A. Fee. (1991). "Kinetic Studies of Superoxide Dismutases: Properties of the Manganese-Containing Protein from *Thermus thermophiles*." *J. Am. Chem. Soc.*, **113**, 4069–4076; (*e*) A. S. Hearn, M. E. Stroupe, D. E. Cabelli, J. R. Lepock, J. A. Tainer, H. S. Nick and D. N. Silverman. (2001). "Kinetic Analysis of Product Inhibition in Human Manganese Superoxide Dismutase." *Biochemistry*, **40**, 12051–12058; (*f*) A. S. Hearn, C. K. Tu, H. S. Nick and D. N. Silverman. (1999). "Characterization of the Product-inhibited Complex in Catalysis by Human Manganese Superoxide Dismutase." *J. Biol. Chem.*, **274**, 24457–24460.

[4] B. Meunier. (1999). *Biomimetic Oxidations Catalyzed by Transition Metal Complexes*, Imperial College Press, London.

[5] D. L. Wertz and J. S. Valentine. (2000). "Nucleophilicity of Iron-Peroxo Prophyring

Complexes." *Struct. Bonding*, **97**, 37–60.

[6] (*a*) A. D. N. Vaz, E. S. Roberts and M. J. Coon. (1991). "Olefin Formation in the Oxidative Deformylation of Aldehydes by Cytochrome P-450. Mechanistic Implications for Catalysis by Oxygen-Derived Peroxide." *J. Am. Chem. Soc.*, **113**, 5886–5887; (*b*) M. Akhtar, D. Corina, S. Miller, A. Z. Shyadehi and J. N. Wright. (1994). "Mechanism of the Acyl-Carbon Cleavage and Related Reactions Catalyzed by Multifunctional P-450s: Studies on Cytochrome P-$450_{17\alpha}$." *Biochemistry*, **33**, 4410–4418.

[7] (*a*) E. G. Kovaleva, M. B. Neibergall, S. Chakrabarty and J. D. Lipscomb. (2007). "Finding Intermediates in the O_2 Activation Pathways of Non-Heme Iron Oxygenases." *Acc. Chem. Res.*, **40**, 475–483; (*b*) M. D. Wolfe and J. D. Lipscomb. (2003). "Hydrogen Peroxide-coupled *cis*-Diol Formation Catalyzed by Naphthalene 1,2-Dioxygenase." *J. Biol. Chem.*, **278**, 829–835; (*c*) A. Bassan, M. R. A. Blomberg and P. E. M. Siegbahn. (2004). "A theoretical study of the *cis*-dihydroxylation mechanism in naphthalene 1,2-dioxygenase." *J. Biol. Inorg. Chem.*, **9**, 439–452; (*d*) M. Tarasev and D. P. Ballou. (2005). "Chemistry of the Catalytic Conversion of Phthalate into Its *cis*-Dihydrodiol during the Reaction of Oxygen with the Reduced Form of Phthalate Dioxygenase." *Biochemistry*, **44**, 6197–6207.

[8] W. Nam. (2007). "High-Valent Iron(IV)-Oxo Complexes of Heme and Non-Heme Ligands in Oxygenation Reactions." *Acc. Chem. Res.*, **40**, 522-531.

[9] D. Kim, Y. S. Heo, P. R. O. de Montellano. (2008). "Efficient catalytic turnover of cytochrome $P450_{cam}$ is supported by a T252N mutation." *Archives of Biochemistry and Biophysics*, **474**, 150-156.

[10] (*a*) M. M. Abu-Omar, A. Loaiza and N. Hontzeas. (2005). "Reaction Mechanisms of Mononuclear Non-Heme Iron Oxygenases." *Chem. Rev.*, **105**, 2227-2252; (*b*) D. T. Gibson, R. E. Parales. (2000). "Aromatic hydrocarbon dioxygenases in environmental biotechnology." *Curr. Opin. Biotechnol.*, **11**, 236.

[11] (*a*) M. Costas, M. P. Mehn, M. P. Jensen and L. Que, Jr.. (2004). "Dioxygen Activation at Mononuclear Nonheme Iron Active Sites: Enzymes, Models, and Intermediates." *Chem. Rev.*, **104**, 939–986; (*b*) J.-J. Girerd, F. Banse and A. J. Simaan.

(2000). “Characterization and Properties of Non-Heme Iron Peroxo Complexes.” *Struct. Bonding*, **97**, 145–177.

[12] J. Cho, S. Jeon, S. A. Wilson, L. V. Liu, E. A. Kang, J. J. Braymer, M. H. Lim, B. Hedman, K. O. Hodgson, J. S. Valentine, E. I. Solomon and W. Nam. (2011). “Structure and reactivity of a mononuclear non-haem iron(III)-peroxo complex.” *Nature*, **478**, 502–505

[13] J. Annaraj, Y. Suh, M. S. Seo, S. O. Kim and W. Nam. (2005). “Mononuclear nonheme ferric-peroxo complex in aldehyde deformylation.” *Chem. Commun.*, 4529–4531.

[14] F. Li, K. K. Meier, M. A. Cranswick, M. Chakrabarti, K. M. V. Heuvelen, E. Münck and L. Que, Jr.. (2011). “Characterization of a High-Spin Non-Heme Fe^{III}-OOH Intermediate and Its Quantitative Conversion to an Fe^{IV}=O Complex.” *J. Am. Chem. Soc.*, **133**, 7256–7259.

[15] (*a*) J. Cho, R. Sarangi and W. Nam. (2012). “Mononuclear Metal-O_2 Complexes Bearing Macrocyclic N-Tetramethylated Cyclam Ligands.” *Acc. Chem. Res.*, **45**, 1321–1330; (*b*) J. Cho, R. Sarangi, H. Y. Kang, J. Y. Lee, M. Kubo, T. Ogura, E. I. Solomon and W. Nam. (2010). “Synthesis, Structural, and Spectroscopic Characterization and Reactivities of Mononuclear Cobalt(III)-Peroxo Complexes.” *J. Am. Chem. Soc.*, **132**, 16977–16986; (*c*) J. Cho, H. Y. Kang, L. V. Liu, R. Sarangi, E. I. Solomon and W. Nam. (2013). “Mononuclear nickel(II)-superoxo and nickel(III)-peroxo complexes bearing a common macrocyclic TMC ligand.” *Chem. Sci.*, **4**, 1502–1508

[16] (*a*) A. Yokoyama, J. E. Han, J. Cho, M. Kubo, T. Ogura, M. A. Siegler, K. D. Karlin and W. Nam. (2012). “Chromium(IV)-Peroxo Complex Formation and Its Nitric Oxide Dioxygenase Reactivity.” *J. Am. Chem. Soc.*, **134**, 15269–15272; (*b*) H. Kang, J. Cho, K.-B. Cho, T. Nomura, T. Ogura and W. Nam. (2013). “Mononuclear Manganese-Peroxo and Bis(μ-oxo) dimanganese Complexes Bearing a Common N-Methylated Macrocyclic Ligand.” *Chem. Eur. J.*, **19**, 14119–14125; (*c*) D. Kim, J. Cho, Y.-M. Lee, R. Sarangi and W. Nam. (2013). “Synthesis, Characterization, and Reactivity of Cobalt(III)-Oxygen Complexes Bearing a Macrocyclic N-

Tetramethylated Cyclam Ligand." *Chem. Eur. J.*, **19**, 14112–14118.

[17] R. Sarangi, J. Cho, W. Nam and E. I. Solomon. (2011). "XAS and DFT Investigation of Mononuclear Cobalt(III) Peroxo Complexes: Electronic Control of the Geometric Structure in CoO_2 versus NiO_2 Systems." *Inorg. Chem.*, **50**, 614–620.

[18] J. Cho, R. Sarangi, J. Annaraj, S. Y. Kim, M. Kubo, T. Ogura, E. I. Solomon, and W. Nam. (2009). "Geometric and electronic structure and reactivity of a mononuclear 'side-on' nickel(III)-peroxo complex." *Nat. Chem.*, **1**, 568–572.

[19] M. T. Kieber-Emmons, J. Annaraj, M. S. Seo, K. M. V. Heuvelen, T. Tosha, T. Kitagawa, T. C. Brunold, W. Nam and C. G. Riordan. (2006). "Identification of an "End-on" Nickel-Superoxo Adduct, $[Ni(tmc)(O_2)]^+$" *J. Am. Chem. Soc.*, **128**, 14230–14231.

[20] B. M. T. Lam, J. A. Halfen, V. G. Young, Jr., J. R. Hagadorn, P. L. Holland, A. Lledós, L. Cucurull-Sanchez, J. J. Novoa, S. Alvarez and W. B. Tolman. (2000). "Ligand Macrocycle Structural Effects on Copper-Dioxygen Reactivity." *Inorg. Chem.*, **39**, 4059–4072.

[21] S. Hikichi, C. Kobayashi, M. Yoshizawa and M. Akita. (2010). "Tunin the Stability and Reactivity of Metal-bound Alkylperoxide by Remote Site Substitution of the ligand." *Chem. Asian J.*, **5**, 2086–2092.

[22] C. M. Che, Z. Y. Li, K. Y. Wong, C. K. Poon, T. C. W. Mak, S. M. Peng. (1994). "A Simple Synthetic Route To N.N'-Dialdyl-2,11-Diaza[3.3](2,6)-Pyridinophanes. Crystal Structures of N,N'-Di-Tert-Butyl-2,11-Diaza[3.3](2,6)Pyridinophane and Copper(II) Complex." *Polyhedron*, **13**, 771-776.

[23] (*a*) J. R. Khusnutdinova, J. Luo, N. P. Rath and L. M. Mirica. (2013). "Late First-Row Transition Metal Complexes of a Tetradentate Pyridinophane Ligand: Electronic Properties and Reactivity Implications." *Inorg. Chem.*, **52**, 3920−3932; (*b*) B. Zheng, F. Tang, J. Luo, J. W. Schultz, N. P. Rath and L. M. Mirica. (2014). "Organometallic Nickel(III) Complexes Relevant to Cross-Coupling and Carbon-Heteroatom Bond Formation Reactions." *J. Am. Chem. Soc.*, **136**, 6499−6504.

[24] *Purification of Laboratory Chemicals*; W. L. F. Armarego and D. D. Perrin, Eds.;

Pergamon Press: Oxford, 1997.

[25] D. F. Evans. (1959). "The Determination of the Paramagnetic Susceptibility of Substances in Solution by Nuclear Magnetic Resonance." *J. Chem. Soc.*, 2003-2005.

[26] J. Lölinger, R. Scheffold. (1972). "Paramagnetic Moment Measurements by NMR." *J. Chem. Educ.*, **49**, 646-647.

[27] D. F. Evans, D. A. Jakubovic. (1988). "Water-soluble Hexadentate Schiff-base Ligands as Sequestrating Agents for Iron(III) and Gallium(III)." *J. Chem. Soc. Dalton Trans*, 2927-2933.

[28] G. Koz, N. Özdemir, D. Astley, M. Dincer, S. T. Astley. (2010). "Synthesis, spectroscopic and structural characterization of cobalt(II) complex with uracil-containing 2,6-diformylpyridine ligand: Theoretical studies on the ligand and pentagonal-bipyramidal $[Co(L)(H_2O_2)]^{2+}$ and $[Zn(L)(H_2O_2)]^{2+}$." *J. Mol. Struct.*, **966**, 39-47.

[29] Sheldrick, G. M. *SHELXTL/PC*. Version 6.12 for Windows XP; Bruker AXS Inc.; Madison, WI, 2001.

[30] R. I. Haines and A. McAuley. (1981). "Synthesis and Reactions of Nickel(III) Complexes." *Coord. Chem. Rev.*, **39**, 77–119.

[31] S. Graham-Lorence, B. Amarneh, R. E. White, J. A. Peterson and E. R. Simpson. (1995). "A three-dimensional model of aromatase cytochrome P450." *Protein Sci.*, **4** 1065–1080.

[32] M. S. Seo, J. Y. Kim, J. Annaraj, Y. Kim, Y.-M. Lee, S.-J. Kim, J. Kim and W. Nam. (2007). "$[Mn(tmc)(O_2)]^+$: A Side-On Oeroxido Manganese(III) Complex Bearing a Non-Heme Ligand." *Angew. Chem. Int. Ed*, **46**, 377–380.

[33] Y. Jo, J. Annaraj, M. S. Seo, Y.-M. Lee, S. Y. Kim, J. Cho and W. Nam. (2008). "Reactivity of a cobalt(III)-peroxo complex in oxidative nucleophilic reactions." *J. Inorg. Biochemistry*, **102**, 2155–2159.

[34] Unpublished paper in our lab.

[35] Unfortunately, we could not observe the ^{18}O-shifted band of **1** despite our great

efforts. Because it was difficult to fully generate the ^{18}O-labeled **1** with 0.89% of $H_2{}^{18}O_2$. However, we confirmed that the *ν*(O-O) band disappeared when the solution was allowed to warm.

[36] Although we have not been able to determine the structure of **2**, the orientation and the degree of steric property of the cyclohexyl groups around Ni center may be deduced by the structure of $[Ni(CHDAP)(NO_3)](NO_3)(CH_3OH)$ (Fig. 5).

Part II.

Synthesis, Characterization and Reactivity of a Mononuclear Nickel(III)-O_2 Complex with Macrocyclic Ligand, Me_3-TPADP

I. Introduction

Oxygen-including mononuclear metal complexes conduct to important role in the variety of catalytic cycles. To understand the mechanism of dioxygen activation was one of the goal in biomimetic research.[1] Biomimetic compounds of oxygen-containing metal intermediate have been structurally and spectroscopically characterized and investigated in nucleophilic and electrophilic oxidation reactions.[2-8]

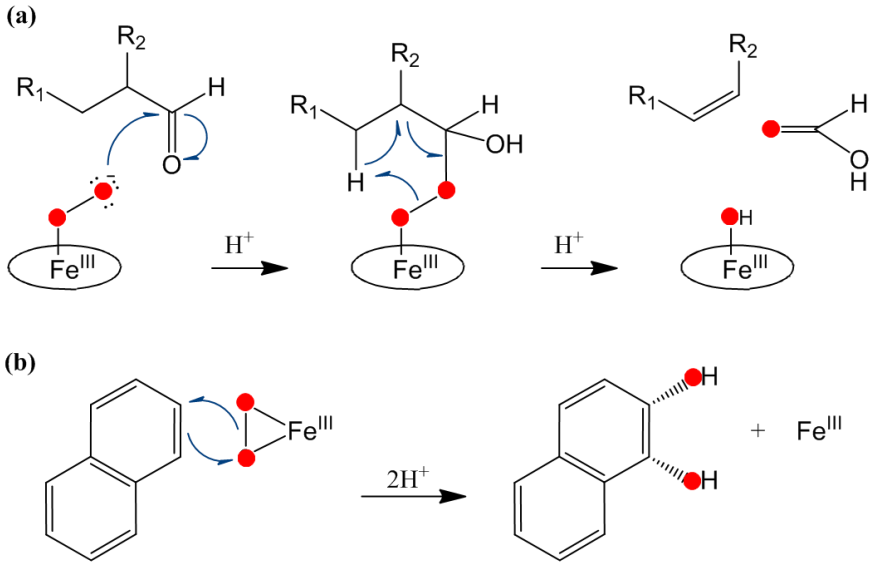

Scheme 9. Proposed Fe(III)-peroxo intermediate in (a) P450 reaction and (b) Rieske Dioxygenase.

For example, ferric-peroxo species with heme and nonheme ligands have been proposed as key intermediate in the chemical models of cytochrome P450 where peroxide complex can act as nucleophilic reaction with aldehydes (Scheme 9a).[3,9-12] In the Rieske Dioxygenase, the O-O bond of Fe(III)-peroxo species activate naphthalene by observing proton (Scheme 9b).[9,13] In addition, the nickel containing enzyme, nickel superoxide dismutase, urease, Ni-Fe hydrogenase, CO dehydrogenase, and methyl-CoM reductase, were attractive.[14a] Among

them, the nickel superoxide dismutase (Ni-SOD) catalyze the dismutation of superoxide (Scheme 10).[14b]. Active oxygen, superoxide, occur from stress, food additives, chemical, and air pollution and induce the cell damage, aging, and disease.

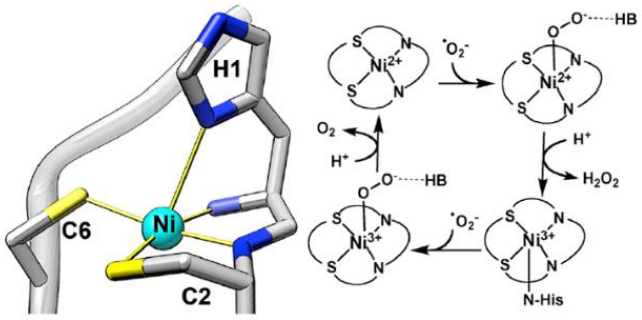

Scheme 10. Ni-SOD active site structure and mechanism.

Recently, the model complexes with various metals (*i.e.* chromium, manganese, iron, cobalt, nickel) with tetraazamacrocyclic *n*-TMC (*n* = 12, 13, 14) ligands have been synthesized, investigated for structure, and confirmed the reactivity properties depending on ring size of ligand.[15] In This work, the Me_3-TPADP (3,6,9-trimethyl-3,6,9-triaza-1(2,6)-pyridinacyclodecaphane), derived from 12-TMC which gives an electronically tunable site on the *para* position of the pyridyl group, was produced (Scheme 9). The *para* position of the pyridyl group in target ligand can substituted with electron withdrawing (Br, Cl) or donating group (Me, OMe).

Here, the starting complex, $[Ni^{II}(Me_3\text{-TPADP})(CH_3CN)_2]^{2+}$ (**3**), and Ni-O_2 intermediate, $[Ni^{III}(Me_3\text{-TPADP})(O_2)]^{+}$ (**4**), were prepared and successfully characterized by various physicochemical methods. The reactivity of **4** toward external organic substrates was identified and then was compared with those of the previously reported Ni-O_2 complexes.

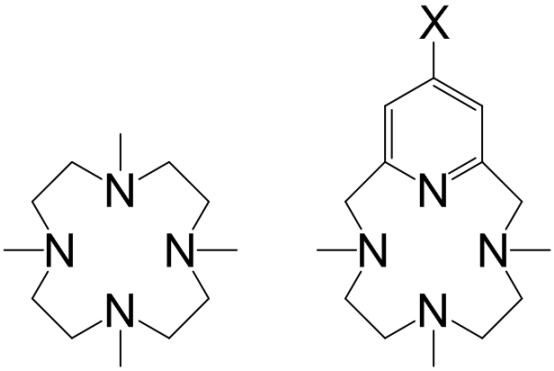

Scheme 11. 12-TMC (left) and Me_3-TPADP (right) (X = H, Cl, Br, Me, OMe)

II. Experimental Section

II-1. Materials and Instrumentation

All chemicals obtained from Aldrich Chemical Co. were the best available purity and used without further purification unless otherwise indicated. Solvents were dried according to published procedures and distilled under Ar prior to use.[16] $H_2{}^{18}O_2$ (90% ^{18}O-enriched, 2% $H_2{}^{18}O_2$ in water) was purchased from ICON Services Inc. (Summit, NJ, USA). The Me_3-TPADP (3,6,9-trimethyl-3,6,9-triaza-1(2,6)-pyridinacyclodecaphane) was little altered[17] and synthetic method was added in this system.

UV-vis spectra were recorded on a Hewlett Packard 8453 diode array spectrophotometer equipped with a UNISOKU Scientific Instruments for low-temperature experiments or with a circulating water bath. Electrospray ionization mass spectra (ESI-MS) were collected on a Waters (Milford, MA, USA) Acquity SQD quadrupole Mass instrument, by infusing samples directly into the source using a manual method. The spray voltage was set at 2.5 kV and the capillary temperature at 80 °C. Resonance Raman spectra were obtained using a liquid nitrogen cooled CCD detector (CCD-1024×256-OPEN-1LS, HORIBA Jobin Yvon) attached to a 1-m single polychromator (MC-100DG, Ritsu Oyo Kogaku) with a 1200 groovs/mm holographic grating. An excitation wavelength of 441.6-nm was provided by a He-Cd laser (Kimmon Koha, IK5651R-G and KR1801C), with 20 mW power at the sample point. All measurements were carried out with a spinning cell (1000 rpm) at −20 °C. Raman shifts were calibrated with indene, and the accuracy of the peak positions of the Raman bands was ±1 cm^{-1}. The effective magnetic moments was determined using the modified ^1H NMR method of Evans at room temperature.[18-20] A WILMAD® coaxial insert (sealed capillary) tubes containing the blank acetonitrile-d_3 solvent (with 1.0 % TMS) only was inserted into the normal

NMR tubes containing the complexes dissolved in acetonitrile-d_3 (with 0.03 % TMS). The chemical shift of the TMS peak (and/or solvent peak) in the presence of the paramagnetic metal complexes was compared to that of the TMS peak (and/or solvent peak) in the inner coaxial insert tube. The effective magnetic moment was calculated using the equation, $\mu = 0.0618(\Delta\nu T/2fM)^{1/2}$, where f is the oscillator frequency (MHz) of the superconducting spectrometer, T is the absolute temperature, M is the molar concentration of the metal ion, and $\Delta\nu$ is the difference in frequency (Hz) between the two reference signals. CW-EPR spectra were taken at 5 K using an X-band Bruker EMX-plus spectrometer equipped with a dual mode cavity (ER 4116DM). Low temperatures were achieved and controlled using an Oxford Instruments ESR900 liquid He quartz cryostat with an Oxford Instruments ITC503 temperature and gas flow controller. Product analysis was performed with an Agilent Technologies 6890N gas chromatograph (GC) and Thermo Finnigan (Austin, Texas, USA) FOCUS DSQ (dual stage quadrupole) mass spectrometer interfaced with Finnigan FOCUS gas chromatograph (GC-MS). ^{1}H NMR and ^{13}C-NMR spectra were measured with Bruker AVANCE III-400 spectrometer.

II-2. Synthesis of Ligands

II-2-a. 1,4,7-tris(*p*-tosylsulfonyl)-1,4,7-triazaheptane (L4).

To a Diethylentriamine (4.7 mL, 44 mmol) in Acetone in an ice bath, K_2CO_3 (18.2 g) in water and p-toluensulfonyl chloride (25.2 g) in acetone were added slowly. After the ice bath was removed, the mixture was stirred for 3 hours. The mixture was added to an ice water with stirring. The mixture was filtered and then the final powder was formed by washing with water. Yield: 13.19 g (53 %), ^{1}H NMR ($CDCl_3$, 400 MHz): 2.38 (9H, s, CH_3), 2.81 (4H, t, CH_2), 3.02 (4H, t, CH_2), ~7.53 (12H, m, PyH)

II-2-b. 3,6,9-tris(p-tosylsulfonyl)-3,6,9,15-tetraazbicyclo[9,3,1]pentadeca-1(15), 11, 13 -triene (L5).

A DMF solution of **L3** (2.2 g, 8.3 mmol) was slowly added to a DMF solution of **L4** (4.7 g, 8.3 mmol) and K_2CO_3 (1.147 g, 8.3 mmol) with stirring for overnight. The ice water was added to the mixture and then white solid was formed by filteration and washed with water and EtOH. Yield: 3.44 g (62 %), ^{1}H NMR ($CDCl_3$, 400 MHz): 2.45 (9H, s, CH_3), 2.75 (4H, d, CH_2), 3.32 (2H, d, CH_2), 4.29 (4H, s, CH_2), ~7.6 (15H, m PyH)

II-2-c. 3,6,9,15-tetraazabocyclo(9,3,1)pentadeca-1(15),11,13-triane (L6).

L5 (0.6 g, 0.897 mmol) was refluxed with H_2SO_4 (5 mL, 44.85 mmol) for 2 hours then cooled to room temperature. The reaction mixture was treated with NaOH solution and then separated with chloroform and dried over Na_2SO_4. Solvent was removed by rotary evaporation to afford the powder. Yield: 0.165g (89 %), ^{1}H NMR ($CDCl_3$, 400 MHz): 2.69 (4H, d, CH_2), 2.24 (4H, d, CH_2), 3.96 (4H, s, CH_2), 7.01 (2H, d, PyH), 7.51 (1H, t, PyH)

II-2-d. 3,6,9-trimethyl-3,6,9-triaza-1(2,6)-pyridinacyclodecaphane (Me_3-TPADP).

The formaldehyde (0.8 mL, 7.64 mmol) and formic acid (0.6 mL, 15.35 mmol) was added to **L6** (0.15 g, 0.727 mmol) in an ice bath and stirred for 1 hour. After cooling to room temperature, the mixture was refluxed for overnight and then treated with NaOH solution. The reaction mixture was separated with CH_2Cl_2 and dried over $MgSO_4$. Solvent was removed and washed with pentane to afford the final oil. Yield: 0.13 g (71 %), ^{1}H NMR ($CDCl_3$, 400 MHz): 2.26 (3H, s, CH_3), 2.48 (6H, s, CH_3), 2.58 (8H, d, CH_2), 3.78 (4H, s, CH_2), 7.11 (2H, d, PyH), 7.59 (1H, t, PyH)

II-3. Generation of Ni Complexes

II-3-a. $[Ni(Me_3\text{-}TPADP)(CH_3CN)_2]^{2+}$ (3).

Me_3-TPADP (0.124 g, 0.5 mmol) in CH_3CN (1 mL) was added to CH_3CN solution (1 mL) of $Ni(ClO_4)_2{\cdot}6H_2O$ (0.18 g, 0.5 mmol). The resulting solution was stirred, affording a violet solution. The solvents were removed under vaccum to yield violet powder, which was recrystallized from CH_3CN/Et_2O solution as a violete crystalline product. Crystalline yield: 0.2 g (86%). UV-vis (CH_3CN): λ_{max} (ε) = 541 nm (16 M^{-1} cm^{-1}) and 904 nm (31 M^{-1} cm^{-1}). ESI-MS (CH_3CN): *m/z* 173.6 for $[Ni(Me_3\text{-}TPADP)(CH_3CN)]^{2+}$, and 194.1 for $[Ni(Me_3\text{-}TPADP)(CH_3CN)_2]^{2+}$, and 405.2 for $[Ni(Me_3\text{-}TPADP)(ClO_4)]^{+}$. Anal. Calcd for $C_{18}H_{32}N_6Cl_2NiO_9$ ($[Ni(Me_3\text{-}TPADP)(CH_3CN)_2](ClO_4)_2(H_2O)$): C, 35.67; H, 5.32; N, 13.87. Found: C, 35.13; H, 5.134; N, 13.45. μ_{eff} = BM. X-ray crystallographically suitable crystals were obtained by slow diffusion of Et_2O into CH_3CN solution of **3**. The magnetic moment of 3.1 μ_B,[21] determined using the ^1H NMR Evans method, is consistent with an S =1 ground state of **3**.

II-3-b. Generation and Characterization of $[Ni(Me_3\text{-}TPADP)(O_2)]^{+}$ (4).

Treatment of $[Ni(Me_3\text{-}TPADP)(CH_3CN)_2](ClO_4)_2$ (2 mM) with 5 equiv. H_2O_2 in the presence of 2 equiv. of TEA in CH_3CN (2 mL) at 25 ℃ afforded a greenish blue solution. Spectroscopic data, including UV-vis, ESI-MS, resonance Raman, and EPR, were reported in 'Result and Discussion' section. $[Ni(Me_3\text{-}TPADP)(^{18}O_2)]^{+}$ was prepared by adding 5 equiv. of $H_2{}^{18}O_2$ (36 μL, 90% ^{18}O-enriched, 2% $H_2{}^{18}O_2$ in water) to a solution containing $[Ni(Me_3\text{-}TPADP)(CH_3CN)_2](ClO_4)_2$ (2 mM) and 2 equiv. of TEA in CH_3CN (2 mL) at ambient

temperature. UV-vis (CH_3CN): λ_{max} (ε) = 345 nm (224 M^{-1} cm^{-1}), 569 nm (30 M^{-1} cm^{-1}), and 904 nm (40 M^{-1} cm^{-1}). ESI-MS (CH_3CN): 494.2 for $[Ni(CHDAP)(O_2)]^+$.

II-4. X-ray Crystallography

Single crystals of $[Ni(Me_3\text{-}TPADP)(CH_3CN)_2](ClO_4)_2$ was picked from solutions by a nylon loop (Hampton Research Co.) on a hand made copper plate mounted inside a liquid N_2 Dewar vessel at *ca*. –40 ℃ and mounted on a goniometer head in a N_2 cryostream. Data collections were carried out on a Bruker SMART APEX II CCD diffractometer equipped with a monochromator in the Mo Kα (λ = 0.71073 Å) incident beam. The CCD data were integrated and scaled using the Bruker-SAINT software package, and the structure was solved and refined using SHELXTL V 6.12.[21] Hydrogen atoms were located in the calculated positions. All non-hydrogen atoms were refined with anisotropic thermal parameters.

II-5. Reactivity Studies

Reactions of **4** was run in a 1-cm UV cuvette by monitoring UV-vis spectral changes of reaction solutions in CH_3CN. Rate constants were determined by fitting the changes in absorbance at 342 nm for $[Ni^{III}(Me_3\text{-}TPADP)(O_2)]^+$ (**4**) at –10℃. Reactions were carried out at least in triplicate, and the data reported represent the average of these reactions. After the completion of reactions, pseudo-first-order fitting of the kinetic data allowed us to determine k_{obs} values.

Product formed in the oxidation of CCA by **4** in CH_3CN at –10 ℃ was analyzed by GC and GC-MS. Product was analyzed by injecting the reaction mixture directly into HPLC and GC, GC-MS. Products were identified by comparing with authentic samples, and product yield was determined by comparison against standard areas prepared with authentic sample (using decane as an internal standard).

III. Results and Discussion

III-1. Synthesis and Characterization of Me_3-TPADP

The Me_3-TPADP (3,6,9-trimethyl-3,6,9-triaza-1(2,6)-pyridinacyclodecaphane) ligand was synthesized through the several steps and synthetic method was shown in scheme 12. The final product was obtained and characterized by ESI-MS (Fig. 15). The ESI-MS of Me_3-TPADP exhibits a ion peak at a mass-to-charge ratio of 249.39 (calculated *m/z* of 249.21). Inset shows an observed isotope distribution pattern for $[Me_3\text{-TPADP} + H]^+$.

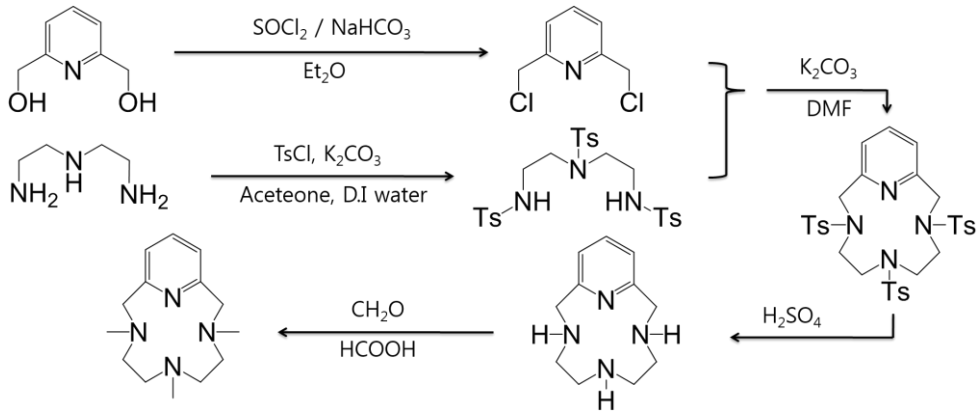

Scheme 12. Synthetic routes for 3,6,9-trimethyl-3,6,9-triaza-1(2,6)-pyridinacyclodecaphane (Me_3-TPADP).

The sticky Me_3-TPADP ligand was formed well in good quality through a number of efforts and steps (Fig. 16). The target ligand in $CDCl_3$ was characterized by ^1H NMR at room temperature (Fig. 17).

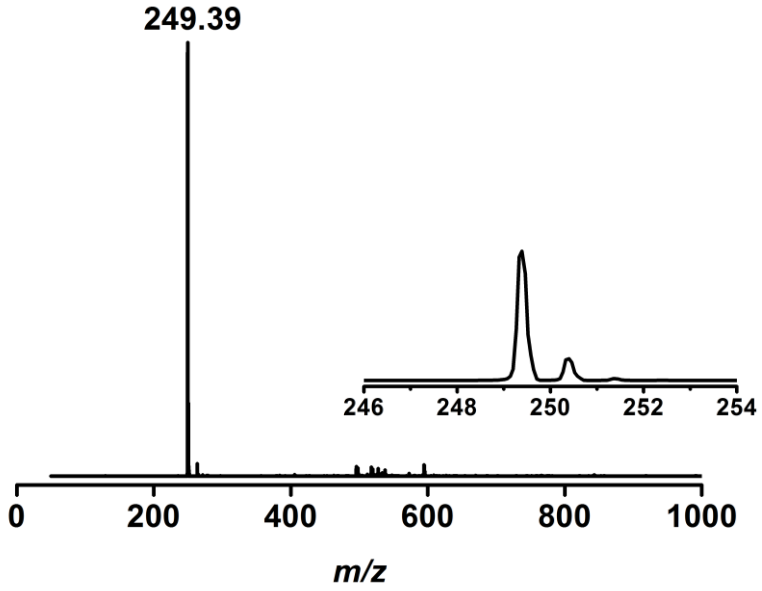

Figure 15. ESI-MS for the Me_3-TPADP ligand in CH_3CN. Inset shows an observed isotope distribution pattern for [Me_3-TPADP + H]$^+$.

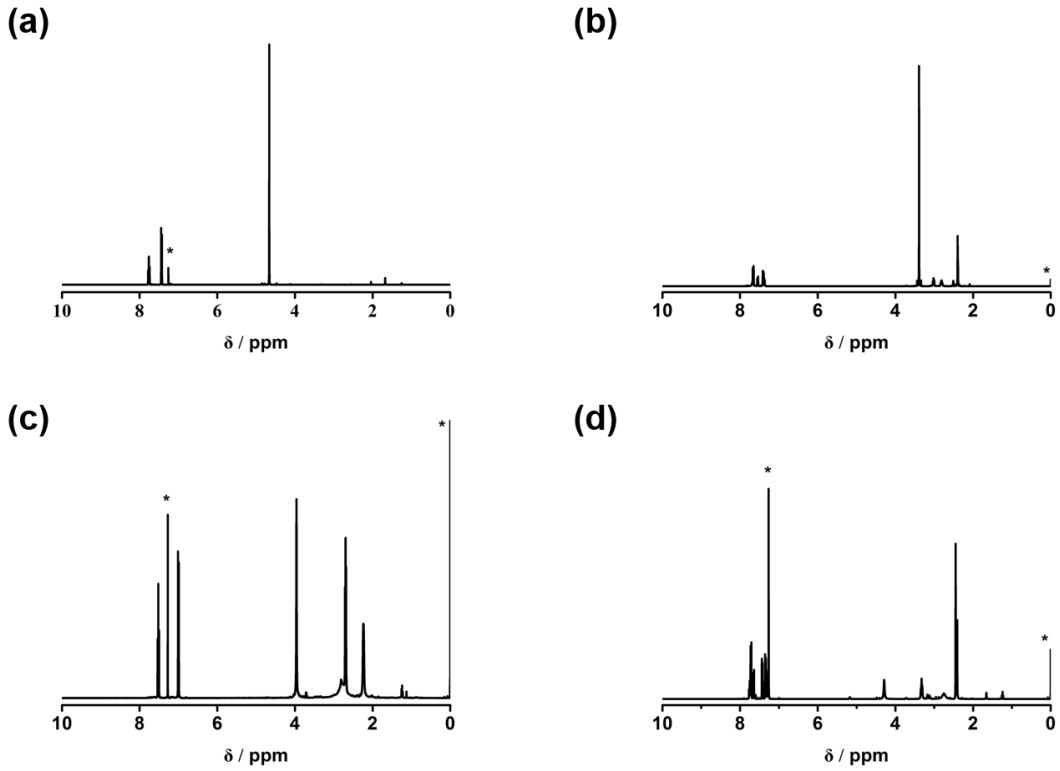

Figure 16. The ^{1}H NMR result of (a) **L3**, (b) **L4**, (c) **L5**, and (d) **L6**. The asterisk is a solvent or tetramethylsilane (TMS) peak and highest peak of (b) is H_2O.

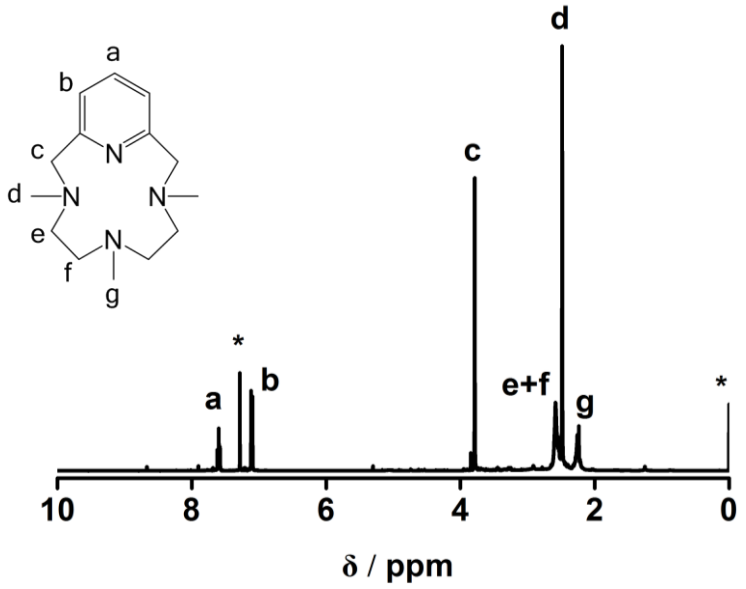

Figure 17. ^{1}H NMR spectrum of the Me_3-TPADP ligand in $CDCl_3$ at room temperature. The asterisk is a solvent band.

III-2. Preparation and Characterization $[Ni^{II}(Me_3\text{-}TPADP)(CH_3CN)_2]^{2+}$ (3)

The complex **3** was synthesized by reacting with $Ni(ClO_4)_2{\cdot}6H_2O_2$ and Me_3-TPADP in CH_3CN at room temperature; the color of the complex **3** solution is violet. The UV-vis spectrum of **3** in CH_3CN at 25 ℃ appears broad bands at 541 nm (ε = 33 M^{-1} cm^{-1}) and 905 nm (ε = 61 M^{-1} cm^{-1}) (Fig. 20).

The ESI-MS of **3**, which recrystallized with CH_3CN/Et_2O, show intense peaks at a mass-to-charge (*m/z*) ratio of 173.6, 194.1, and 405.2 for $[Ni(Me_3\text{-}TPADP)(CH_3CN)]^{2+}$ (calculated *m/z* of 173.58), $[Ni(Me_3\text{-}TPADP)(CH_3CN)_2]^{2+}$ (calculated *m/z* of 194.095), and $[Ni(Me_3\text{-}TPADP)(ClO_4)]^{+}$ (calculated *m/z* of 405.08), respectively (Fig. 18).

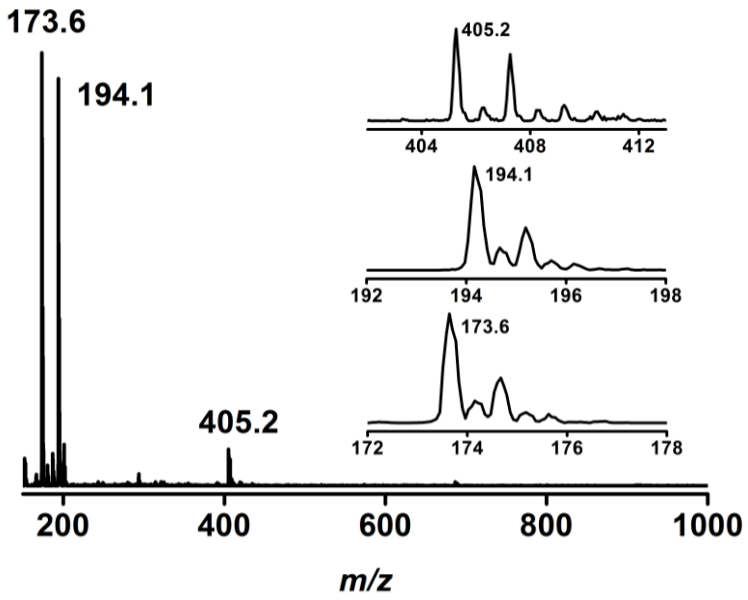

Figure 18. ESI-MS for $[Ni^{II}(Me_3\text{-TPADP})(CH_3CN)_2]^{2+}$ in CH_3CN. Mass peaks at 173.6, 194.1 and 405.2 are assigned to $[Ni(Me_3\text{-TPADP})(CH_3CN)]^{2+}$, $[Ni(Me_3\text{-TPADP})(CH_3CN)_2]^{2+}$ and $[Ni(Me_3\text{-TPADP})(ClO_4)]^{+}$, respectively.

The crystal of **3** was generated in CH_3CN/Et_2O. The structure of cationic part is shown in Fig. 19. X-ray structure of $[Ni^{II}(Me_3\text{-TPADP})(CH_3CN)_2]^{2+}$ with thermal ellipsoids drawn at the 30% probability level and hydrogen atoms are omitted for clarity. Complex **3**, which is distorted structure, has a six-coordinated Ni(II) ion with four nitrogens of the Me_3-TPADP ligand and two nitrogens of CH_3CN. The 2 unit of complex **3**, 3a and 3b, is described in table 3.

The crystallographic data of selected bond distances and angles for $[Ni(Me_3\text{-TPADP})(CH_3CN)_2](ClO_4)_2$ is shown in Table. 3 and 4. This data can be obtained free of charge via www.ccdc.cam.ac.uk/data_request/cif (or from the Cambridge Crystallographic Data Centre, 12, Union Road, Cambridge CB2 1EZ, UK; fax: (+44) 1223-336-033; or deposit@ccdc.cam.ac.uk).

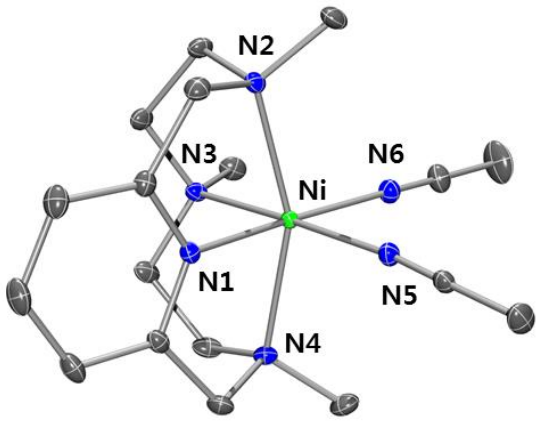

Figure 19. X-ray structure of $[Ni^{II}(Me_3\text{-TPADP})(CH_3CN)_2]^{2+}$ cation in **3**-$(ClO_4)_2$ showing 30% probability thermal ellipsoids. Hydrogen atoms are omitted for clarity.

Table 3. Selected bond distances (Å) and angles (º) for $[Ni(Me_3\text{-TPADP})(CH_3CN)_2](ClO_4)_2$.

Bond Distances (Å)			
3a		3b	
Ni1-N1	1.994(17)	Ni2-N7	1.9898(17)
Ni1-N2	2.1731(17)	Ni2-N8	2.1620(17)
Ni1-N3	2.1433(17)	Ni2-N9	2.1606(18)
Ni1-N4	2.1682(17)	Ni2-N10	2.1650(18)
Ni1-N5	2.0864(18)	Ni2-N11	2.0974(18)
Ni1-N6	2.0229(18)	Ni2-N12	2.0257(18)
Bond Angles (º)			
3a		3b	
N1-Ni1-N2	80.44(7)	N7-Ni2-N8	80.72(7)
N1-Ni1-N3	91.73(7)	N7-Ni2-N9	92.01(7)
N1-Ni1-N4	80.27(7)	N7-Ni2-N10	80.50(7)
N2-Ni1-N3	83.84(7)	N8-Ni2-N9	83.30(7)
N2-Ni1-N4	156.62(7)	N8-Ni2-N10	157.07(7)
N3-Ni1-N4	83.69(7)	N9-Ni2-N10	84.33(7)

Table 4. Crystal data and structure refinements for $[Ni(Me_3\text{-}TPADP)(CH_3CN)_2](ClO_4)_2$.

	$[Ni(CHDAP)(NO_3)](NO_3)(CH_3OH)$
Empirical formula	$C_{18}H_{30}C_{12}N_6NiO_8$
Formula weight	588.09
Temperature (K)	100(2)
Wavelength (Å)	0.71073
Crystal system/space group	Monoclinic, *P21/w*
Unit cell dimensions	
a (Å)	15.7235(4)
b (Å)	19.6733(5)
c (Å)	16.2939(4)
α (°)	90
β (°)	97.9340(10)
γ (°)	90
Volume (Å^3)	4992.0(2)
Z	8
Calculated density (g/cm^{-3})	1.565
Absorption coefficient (mm^{-1})	1.046
Reflections collected	12414
Independent reflections [*R*(int)]	641 [0.0522]
Refinement method	Full-matrix least-squares on F^2
Data/restraints/parameters	12414/0/641
Goodness-of-fit on F^2	1.018
Final *R* indices [$I > 2\text{sigma}(I)$]	$R_1 = 0.0421$ $wR_2 = 0.1099$
R indices (all data)	$R_1 = 0.0473$ $wR_2 = 0.1150$
Largest difference peak and hole (e/Å^3)	1.878 and -1.389

III-3. Characterization and Reactivity Studies of $[Ni^{III}(Me_3\text{-}TPADP)(O_2)]^+$ (**4**)

The reaction of **3** with 5 equiv. of H_2O_2 and 2 equiv. of triethylamine (TEA) in CH_3CN at 25°C produces $[Ni^{III}(Me_3\text{-}TPADP)(O_2)]^+$ (**4**) intermediate. The color of the solution changed from purple to dark blue, which allowed different UV-vis absorption bands at 345 nm (ε = 224 M^{-1} cm^{-1}), 581 nm (ε = 31 M^{-1} cm^{-1}), and 904 nm (ε = 40 M^{-1} cm^{-1}) (Fig. 20).

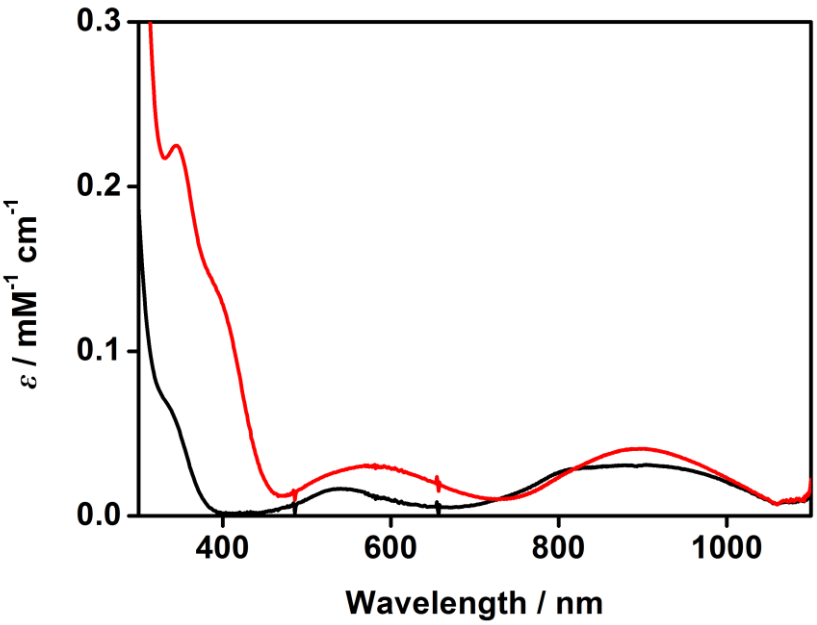

Figure 20. UV-vis spectra of $[Ni^{II}(Me_3\text{-}TPADP)(CH_3CN)_2]^{2+}$ (**3**) (black line) and $[Ni^{III}(Me_3\text{-}TPADP)(O_2)]^+$ (**4**) (red line) in CH_3CN at 25 °C.

The ESI-MS of **4** shows signal at *m/z* of 338.19 (calculated *m/z* of 338.13), whose mass and isotope distribution pattern correspond to $[Ni^{III}(Me_3\text{-}TPADP)(^{16}O_2)]^+$ (**4**-^{16}O). When the reaction was carried out with isotopically labeled $H_2{}^{18}O_2$, a mass peak corresponding to $[Ni^{III}(Me_3\text{-}TPADP)(^{18}O_2)]^+$ (**4**-^{18}O) appeared at *m/z* of 342.23 (calculated *m/z* of 342.13) (Fig. 21). Alternatively, the complex **4** was prepared by different source, KO_2, which was confirmed by distinguished ESI-MS peak (*m/z* of 338.19) and UV-vis.

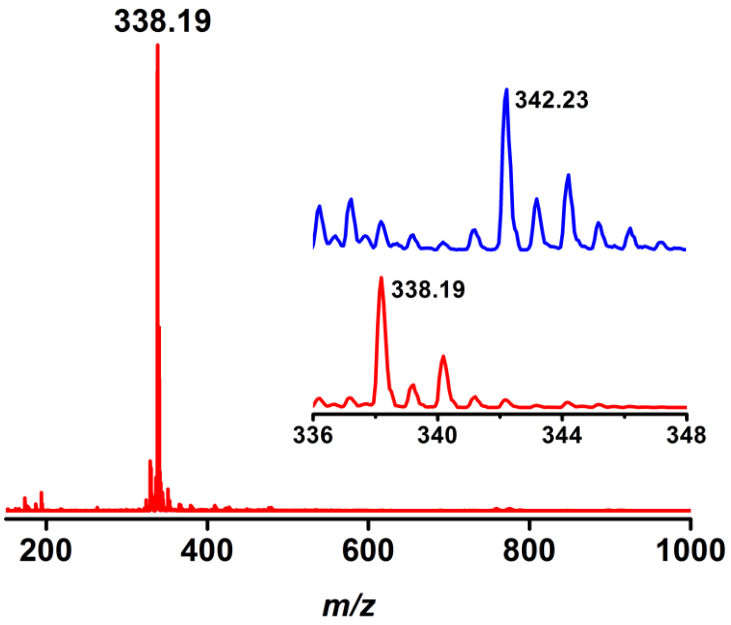

Figure 21. ESI-MS of **4** in CH_3CN at –40 °C. Insets show the observed isotope distribution patterns for $[Ni(Me_3\text{-}TPADP)(^{16}O_2)]^+$ (lower) and $[Ni(Me_3\text{-}TPADP)(^{18}O_2)]^+$ (upper).

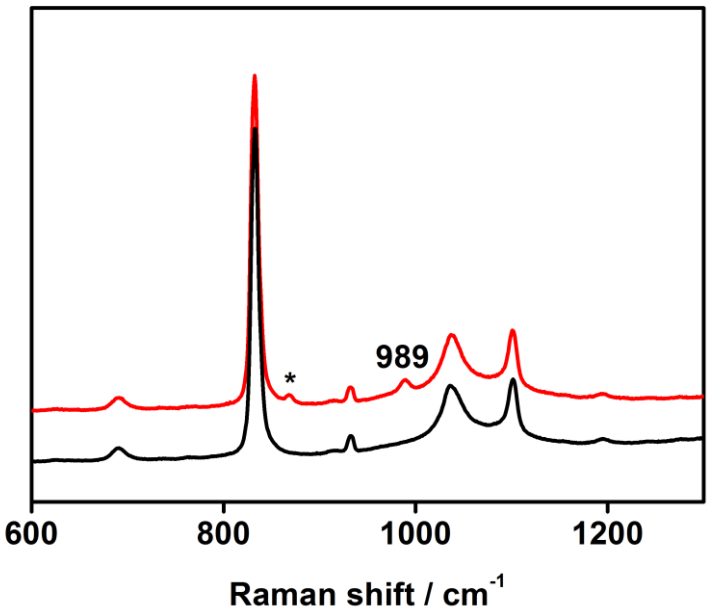

Figure 22. Resonance Raman spectra of **4** (32 mM) obtained upon excitation at 442 nm in CD3CN at -35 °C; red line is **4** which prepared with $H_2{}^{16}O_2$ and black line is decay spectrum of **4**. An asterisk indicates the peak of H_2O_2.

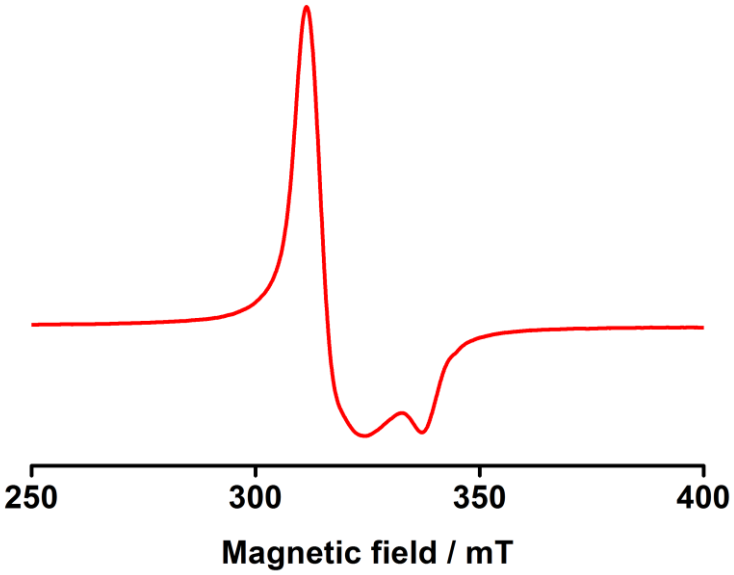

Figure 23. X-band EPR spectrum of **4** in frozen CH_3CN at 5 K. Instrumental parameters: microwave power = 1 mW, frequency = 9.646 GHz, sweep width = 0.15 T, modulation amplitude = 1 mT.

The resonance Raman spectrum of **4** were collected using 442 nm in CH_3CN at -35 ℃, which shows one band at 989 cm^{-1}. This value is very close to that of complex **2** (988 cm^{-1}), $[Ni^{III}(TBDAP)(O_2)]^+$ (989 cm^{-1}), and $[Ni^{III}(12\text{-}TMC)(O_2)]^+$ (1002 cm^{-1}) (Fig. 22).[12a] The EPR spectrum of a frozen CH_3CN solution of **4** at 5 K shows an axial signal with *g* values of 2.18 and 2.04 (Fig. 23), which is indicative of a (S = 1/2) Ni(III) complexes.[22]

The reactivity study of **4** was tested in aldehyde deformylation reaction. The intermediate **4** has been investigated in nucleophilic reaction. Reacting CCA for **4** in CH_3CN at –10 °C, the characteristic UV-vis absorption bands of **4** disappeared with a pseudo-first-order decay (Fig. 24). Product analysis of the reaction solutions revealed the formation of cyclohexene (84%) in the oxidation of CCA. The pseudo-first-order rate constants increased proportionally with substrate concentration which gives second-order rate constant of $k_2 = 9 \times 10^{-2}$ M^{-1} s^{-1} at -10 °C (Fig. 25). The aldehyde deformylation of **4** between 263 and 293 K give

the activation parameters of $\Delta H^{\ddagger}$ = 28 kJ mol^{-1} and $\Delta S^{\ddagger}$ = −174 J mol^{-1} K^{-1} (Fig. 26). The addition of triphenylphosphine or cyclohexadiene to **4**, the intermediate spectrum remains without any change. These results support that **4** have a nucleophilic character.

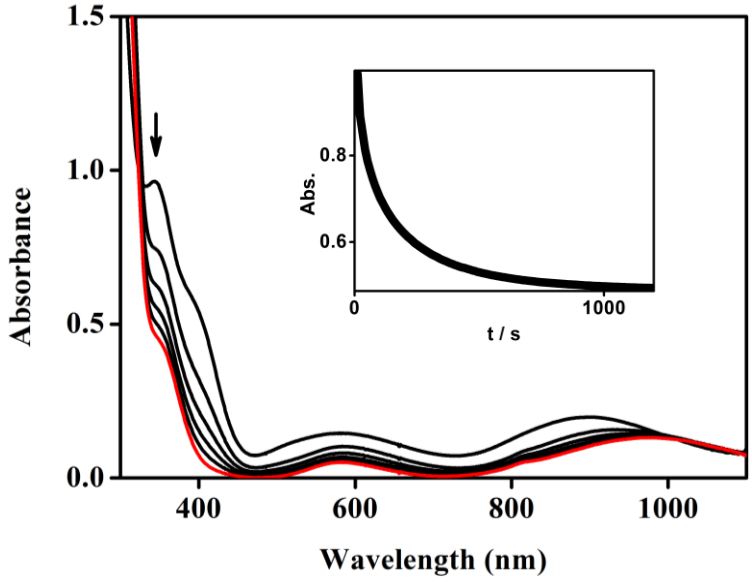

Figure 24. UV-vis spectral changes of [Ni^{III}(Me$_3$-TPADP)(O$_2$)]$^+$ (2) (4 mM) upon addition of 20 equiv. of cyclohexanecarboxaldehyde (CCA) in CH$_3$CN at **–**10 ^{o}C. Inset shows the time course of the absorbance at 342 nm.

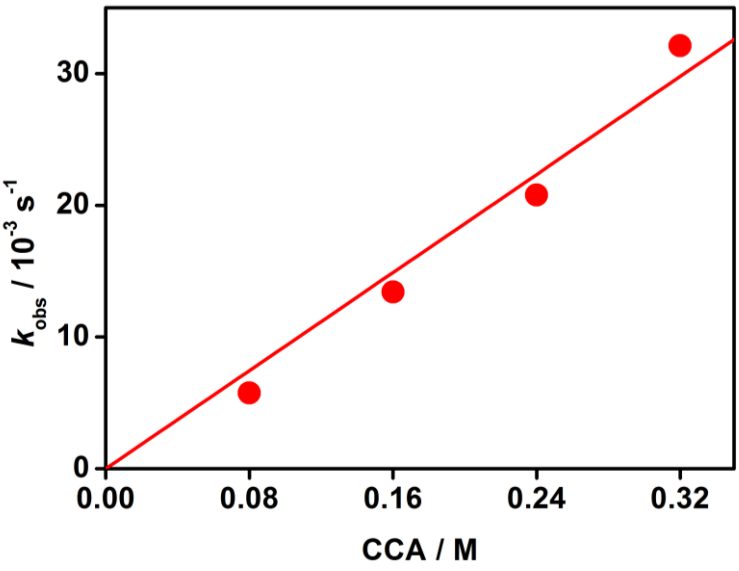

Figure 25. Plots of k_{obs} against CCA concentration to determine a second-order rate constants at **–** 10 °C.

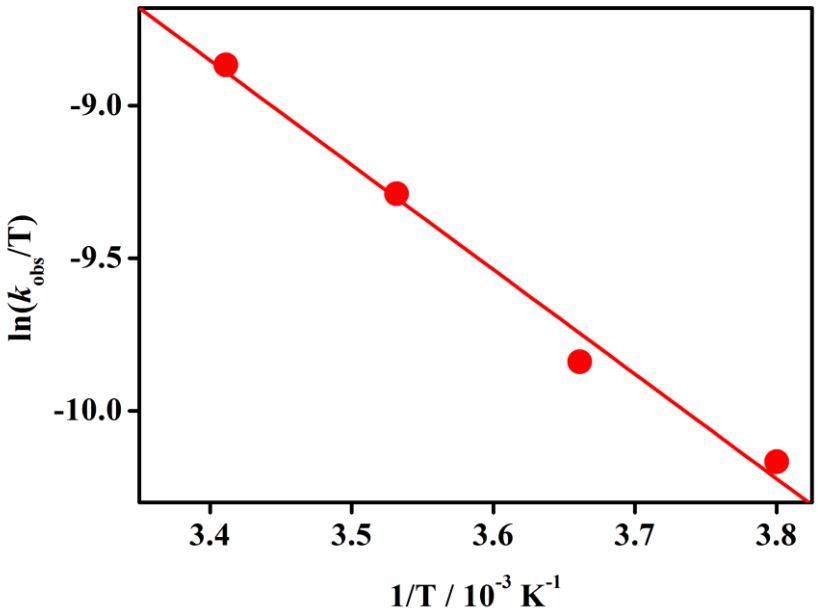

Figure 26. Plot of first-order rate constants against 1/*T* to determine activation parameters.

The $[Ni^{III}(Me_3\text{-TPADP})(O_2)]^+$ (**4**) and $[Ni^{III}(12\text{-TMC})(O_2)]^+$ has similar character. In the resonance Raman spectrum, O-O stretching frequency of complex **4** (988 cm^{-1}**)** was indicated the similar with previous report.[13] The complex **4** was confirmed the Ni(III)-peroxo species from the various experiments in this thesis. Complex **4** have nucleophilic character by aldehyde deformylation reaction with CCA. Kinetic study of the nucleophilic reaction with CCA revealed that **4** (k_2 = 9 × 10^{-2} M^{-1} s^{-1} at -10 °C) and $[Ni^{III}(12\text{-TMC})(O_2)]^+$ (k_2 = 2.0 × 10^{-1} M^{-1} s^{-1} at -10 °C) have no significant difference.[13]

IV. Conclusion

In this thesis, synthesis and characterization of Ni-O_2 complex bearing Me_3-TPADP ligand has been reported. The $[Ni(Me_3\text{-TPADP})(CH_3CN)_2]^{2+}$ (**3**) complex was prepared with $Ni(ClO_4)_2{\cdot}6H_2O$ and Me_3-TPADP ligand in CH_3CN. Complex **3** was identified by UV-vis, ESI-MS, EA, ^1H NMR of Evans, and X-ray methods. The Ni(III)-O_2 complex was generated by reacting with **3** and H_2O_2 in presence of TEA. The intermediate was characterized by UV-vis, ESI-MS, rRaman, and EPR. Intermediate was shown as nucleophilic reaction character by kinetic study with CCA. The reactivity of $[Ni(Me_3\text{-TPADP})(O_2)]^+$ (**4**) with CCA was obtained by UV-vis and has second-order rate constant of $k_2 = 9 \times 10^{-2}$ M^{-1} s^{-1} at –10 °C. Reactivity study of intermediate with organic substrate, give fundamental information into the biomimetic research.

V. References

[1] W. Nam. (2007). "Dioxygen Activation by Metalloenzymes and Models." *Acc. Chem. Res.*, **40**, 465, and review articles in the special issue.

[2] I. M. Klotz and D. M. Jr. Kurtz. (1994). "Metal-Dioxygen Complexes: A perspective." (eds) Special issue on metal-dioxygen complexes. *Chem. Rev.*, **94**, 567–856.

[3] D. L. Wertz and Valentine, J. S. (2000). "Nucleophilicity of Iron-Peroxo Prophyring Complexes." *Struct. Bonding*, **97**, 37–60.

[4] J.-J. Girerd, F. Banse and A. J. Simaan. (2000). "Characterization and Properties of Non-Heme Iron Peroxo Complexes." *Struct. Bonding*, **97**, 145–177.

[5] A. Bakac. (2006). "Kinetic and mechanistic studies of the reactions of transition metal-activated oxygen with inorganic substrates." *Coord. Chem. Rev.*, **250**, 2046–2058.

[6] S. Hikichi, M. Akita and Y. Moro-oka. (2000). "New aspects of the cobalt-dioxygen complex chemistry opened by hydrotris(pyrazoly)borate ligands (Tp^R): unique properties of Tp^RCo-dioxygen complexes." *Coord. Chem. Rev.*, **198**, 61–87.

[7] L. M. Mirica, X. Ottenwaelder and T. D. P. Stack. (2004). "Structure and Spectroscopy of Copper-Dioxygen Complexes." *Chem. Rev.*, **104**, 1013–1045.

[8] E. A. Lewis and W. B. Tolman. (2000). "Reactivity of Dioxygens-Copper Systems." *Chem. Rev.*, **104**, 1047–1076.

[9] k. Ray, F. F. Pfaff, B. Wang and W. Nam. (2014). "Status of Reactive Non-Heme Metal-Oxygen Intermediates in Chemical and Enzymatic Reactions." *J. Am. Chem. Soc.*, Perspective.

[10] (*a*) D. D. LeCloux, A. M. Barrios, S. J. Lippard. (1999). "The Reactivity of Well Defined Diiron(III) Peroxo Complexes Toward Substrates: Addition to Electrophiles and Hydrocarbon oxidation." *Bioorg. Med. Chem. Commun.*, **7**, 763; (*b*) M. Selke, J. S. Valentine. (1998). "Switching on the Nucleophilic Reactivity of

a Ferric Porphyrin Peroxo Complex." *J. Am. Chem. Soc.*, **120**, 2652-2653.

[11] J. Annaraj, Y. Suh, M. S. Seo, S. O. Kim and W. Nam. (2005). "Mononuclear nonheme ferric-peroxo complex in aldehyde deformylation." *Chem. Commun.*, 4529–4531.

[12] (*a*) J. Cho, R. Sarangi, J. Annaraj, S. Y. Kim, M. Kubo, T. Ogura, E. I. Solomon, and W. Nam. (2009). "Geometric and electronic structure and reactivity of a mononuclear 'side-on' nickel(III)-peroxo complex." *Nat. Chem.*, **1**, 568–572; (*b*)) J. Cho, R. Sarangi, H. Y. Kang, J. Y. Lee, M. Kubo, T. Ogura, E. I. Solomon and W. Nam. (2010). "Synthesis, Structural, and Spectroscopic Characterization and Reactivities of Mononuclear Cobalt(III)-Peroxo Complexes." *J. Am. Chem. Soc.*, **132**, 16977–16986.

[13] (*a*) A. Karlsson, J. V. Parales, R. E. Parales, D. T. Gibson, H. Eklund, S. Ramaswamy. (2003). "Crystal Structure of Naphthalene Dioxygenase: Side-On Binding of Dioxygens to Iron." Science, **299**, 1039-1042; (*b*) D. T. Gibson, R. E. Parales. (2000). "Aromatic hydrocarbon dioxygenases in environmental biotechnology." *Curr. Opin. Biotechnol.*, **11**, 236.

[14] (*a*) S. W. Ragsdale. (2007). "Nickel and the carbon cycle." *J. Inorg. Biochem.*, **101**, 1657-1666; (*b*) S. W. Ragsdale. (2009). "Nickel-based Enzyme Systems." *J. Biol. Chem.*, **284**, 18571-18575.

[15] J. Cho, R. Sarangi, W. Nam. (2012). "Mononuclear Metal-O_2 Complexes Bearing Macrocyclic *N*-Tetramethylated Cyclam Ligands." *Acc. Chem. Res.*, **45**, 1321-1330.

[16] *Purification of Laboratory Chemicals*; W. L. F. Armarego and D. D. Perrin, Eds.; Pergamon Press: Oxford, 1997.

[17] J. Wen, S. Geng, Y. Yin, W. Wang. (2012). "A mononuclear Mn^{2+} complex based on a novel tris-(ethyl acetate) pendant-armed tetraazamacrocycle: Effect of pyridine on self-assembly and weak interactions" *Inorg. Chem. Commun.*, **21**, 16-20.

[18] D. F. Evans. (1959). "The Determination of the Paramagnetic Susceptibility of Substances in Solution by Nuclear Magnetic Resonance." *J. Chem. Soc.*, 2003-2005.

[19] J. Lölinger, R. Scheffold. (1972). “Paramagnetic Moment Measurements by NMR.” *J. Chem. Educ.*, **49**, 646-647.

[20] D. F. Evans, D. A. Jakubovic. (1988). “Water-soluble Hexadentate Schiff-base Ligands as Sequestrating Agents for Iron(III) and Gallium(III).” *J. Chem. Soc. Dalton Trans.*, 2927-2933.

[21] Sheldrick, G. M. *SHELXTL/PC*. Version 6.12 for Windows XP; Bruker AXS Inc.; Madison, WI, 2001.

[22] R. I. Haines and A. McAuley. (1981). “Synthesis and Reactions of Nickel(III) Complexes.” *Coord. Chem. Rev.*, **39**, 77–119.

요약문

생체 내 촉매 반응에 있어서 단일 금속-산소 종은 산화 환원 과정의 중요한 중간체 역할을 하기에 많이 연구되어 왔다. 리간드가 금속-산소 복합체의 반응성 패턴에 미치는 영향을 이해하기 위해, 최근, *N*-tetramethylated 거대 고리 킬레이트가 부착된 몇몇 금속-산소 복합체에서 N-리간드의 고리 크기와 반응성 사이의 관계에 대한 체계적인 공부가 진행되었다. 이번 연구에서, CHDAP 그리고 Me_3-TPADP 리간드가 디자인되었고 각각의 리간드가 부착된 니켈-산소 종의 반응성은 part I 그리고 part II에서 각각 조사되었다. 구조적 영향에 따른 반응성의 비교를 위해 형성된 니켈(III)-peroxo 복합체, $[Ni^{III}(CHDAP)(O_2)]^+$ (**2**) 그리고 $[Ni^{III}(TBDAP)(O_2)]^+$, 의 알데하이드 디포밀레이션 반응을 살펴 본 결과, **2** 의 친핵성 반응은 거대고리 리간드의 입체적 성질에 크게 의존하며, 반응성은 $[Ni^{III}(TBDAP)(O_2)]^+$ < $[Ni^{III}(CHDAP)(O_2)]^+$ 임을 알 수 있었다. 이 결과는 구조(입체) 의 방법을 통한 근본적인 통찰력을 준다-금속-peroxo 중간체의 반응성 관계. Part II에서는, Me_3-TPADP 리간드를 합성하였고 $[Ni^{II}(Me_3\text{-}TPADP)(CH_3CN)_2]^{2+}$ (**3**) 와 $[Ni^{III}(Me_3\text{-}TPADP)(O_2)]^+$ (**4**)를 준비 및 특징화하였다. 또한, **4**의 반응성 결과는 외부 기질을 사용하여 얻을 수 있었다.